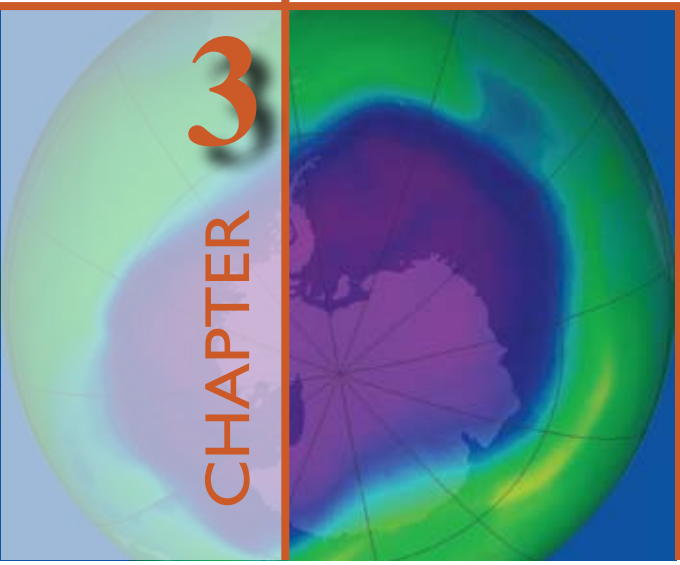

CHAPTER 3

Ozone and UV Observations

Convening Lead Authors: Paul A. Newman, NASA; Jay R. Herman, NASA

Lead Authors: Richard Bevilacqua, NRL; Richard Stolarski, NASA; Terry Keating, U.S. EPA

KEY ISSUES

As atmospheric concentrations of ozone-depleting substances change as a result of implementation of international policies, concentrations of stratospheric ozone and levels of ultraviolet radiation reaching the Earth's surface should also change. However, ozone concentrations and ultraviolet (UV) levels are affected by other natural and human processes as well. To understand whether the international policies are working, we must be able to determine changes in stratospheric ozone and ground-level UV and separate out the effects of ozone-depleting substances (ODS) changes and the effects of other factors.

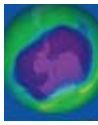

Stratospheric ozone depletion is a global problem that has its most profound effects in the polar regions. However, the processes that drive stratospheric ozone depletion in the polar regions are somewhat different than those that drive depletion in the rest of world. Therefore, the impact of ODS changes may be different in polar regions than over the midlatitude United States.

In this chapter, we briefly review the observations and current understanding and uncertainties in long-term trends in atmospheric ozone and ground-level UV radiation to address the following questions:

- What is the current state of ozone in the stratosphere in the Earth's midlatitudes and over the polar regions?
- What do the observations indicate about the abundances and trends of stratospheric ozone over the United States and elsewhere?
- How do midlatitude ozone levels and the processes that drive them differ from ozone levels and driving processes in the polar regions?
- What is the trend in the occurrence, depth, duration, and extent of the Antarctic ozone hole?
- What is the state of stratospheric ozone depletion in the Arctic region?
- How well do we understand the chemical and meteorological processes that determine stratospheric ozone concentrations in the polar regions and midlatitudes?
- How have UV radiation levels at the Earth's surface in the United States and elsewhere changed as a result of changes in stratospheric ozone?

KEY FINDINGS

- Total global ozone has remained relatively constant over the last four years (2002-2006). Northern midlatitude ozone reached a minimum in 1993 because of forcings from the Mt. Pinatubo eruption and the solar cycle minimum, and has increased somewhat since then. Southern midlatitude ozone decreased until the late 1990s, and has been constant since. There are no significant ozone trends over the tropics.
- Ozone over the continental United States has followed the behavior of ozone for the entire northern midlatitude region; a decrease to a minimum in 1993, and an increase since then (see previous bullet).
- Ozone depletion in the upper stratosphere has closely followed the trends in chlorine. The slow down of the negative (or decreasing) trend is attributed to the leveling off of chlorine in this region of the stratosphere.
- Over the last decade (1995-2006), the Antarctic ozone hole has not worsened. Most Antarctic ozone hole diagnostics show losses leveling off after the mid-1990s. Saturation of ozone loss inside the ozone hole due to complete ozone destruction over a broad vertical layer plays the major role in this leveling off. This complete ozone destruction over a deep vertical layer is modulated by year-to-year dynamical variations. Antarctic ozone hole diagnostics showed an increase of ozone levels in some recent winter years (*e.g.*, 2002, 2004), but these increases resulted from higher levels of dynamical forcing which warmed the Antarctic stratosphere, and not decreases in Equivalent Effective Stratospheric Chlorine levels. In contrast, the Austral spring of 2006 had below average dynamical forcing resulting in below average Antarctic temperatures, causing the 2006 Antarctic ozone hole to be one of the largest on record.
- Arctic spring total ozone values over the last decade were lower than values observed in the 1980s. In addition, spring Arctic ozone is highly variable depending on dynamical conditions. For current halogen levels, anthropogenic chemical loss and variability in ozone transport are about equally important for year-to-year Arctic ozone variability. Colder-than-average vortex conditions result in larger halogen-driven chemical ozone losses. Warmer-than-average vortex conditions result in smaller halogen-driven chemical ozone losses. Variability of temperatures and ozone transport are correlated because they are both driven by dynamic variability.
- Erythemal irradiance (which is a weighted combination of UVA and UVB based on skin sensitivity) over the United States increased roughly by 7% when the ozone minimum was reached in 1993 and is now about 4% higher than in 1979.
- Ground-based measurements of UV irradiance can detect UV trends related to ozone change when data from only days with clear sky are used by correcting for aerosol scattering and absorption using measured aerosol data.
- UV irradiance estimated from satellite data are usually 10% to 30% too high because satellite algorithms neglect the effects of absorbing aerosols.
- UVB irradiance trends can be estimated directly from satellite-measured ozone changes since regional cloud cover and aerosol loadings have not undergone large changes since 1979 except for a short period after the June 1991 Mt. Pinatubo eruption.
- Increased adverse human health effects associated with excessive UV exposure have been observed in Australia, where there are lower ozone amounts and less cloud cover, compared with similar latitudes in the United States.

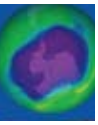

3.1 INTRODUCTION

Ozone is a trace constituent of the atmosphere, with maximum volume mixing ratios of about 10 to 12 molecules per million air molecules (*i.e.*, 10 to 12 ppm). Figure 3.1 (top) shows the annually averaged, longitude-averaged ozone distribution.

The total amount of ozone (*i.e.*, the vertical integral of ozone density from the surface to space) is highest in the mid-to-high latitudes. The bottom panel of Figure 3.1 shows the total ozone integrated from the top panel. In midlatitudes, ozone density is highest in the lower stratosphere between 12 and 25 km (Figure 3.1 middle panel). While the maximum of the ozone mixing ratio (Figure 3.1 top panel) is highest in the tropics at 32 km, the total column ozone is highest in the midlatitudes, not in the tropics (illustrated in the bottom panel).

The distribution of ozone mixing ratios (Figure 3.1 top), density (Figure 3.1 middle), and total ozone (Figure 3.1 bottom) is controlled by the photochemical production, catalytic destruction, and transport. The basic circulation (shown as the yellow streamlines in the upper two panels of Figure 3.1) is known as the Brewer-Dobson circulation (Shepherd, 2007). This Brewer-Dobson circulation carries air into the stratosphere in the tropics near 16 km, leading to very low ozone in the tropical lower stratosphere as the low ozone air is carried upward from the troposphere. The poleward and downward flow of ozone from the tropics produces the midlatitude maximum in both hemispheres.

As air rises in the tropical stratosphere, ozone is produced when molecular oxygen (O_2) is split by solar ultraviolet radiation ($h\nu$) to form oxygen atoms (O) that combine with O_2 in the presence of a third air molecule (M) to form O_3.

$$O_2 + h\nu \rightarrow O + O \quad (1a)$$

$$2\,(O + O_2 + M \rightarrow O_3 + M) \quad (1b)$$

Net: $3\,O_2 + h\nu \rightarrow 2\,O_3$

This solar production of ozone leads to very high ozone concentrations in the mid-stratosphere in the tropics (near 32 km).

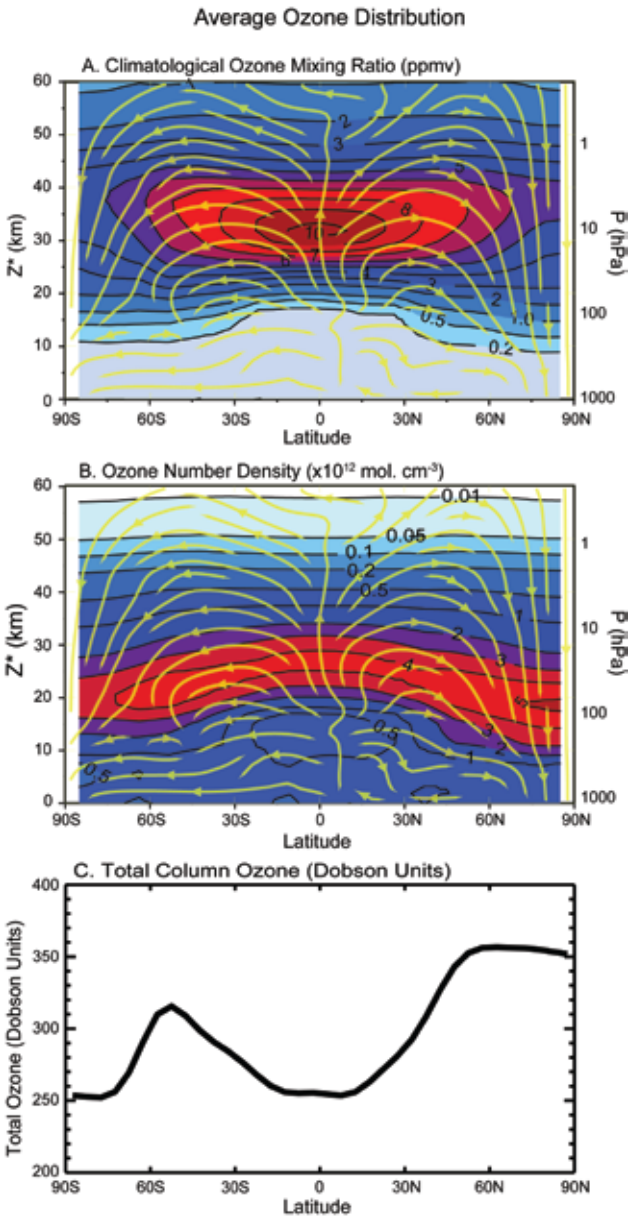

Figure 3.1 Annual longitudinal averaged ozone mixing ratios (top), ozone density (middle), and annual longitudinal averaged total ozone (bottom). Top panel units are parts per million (ppm); middle panel units are molecules per cm^3; bottom panel units are Dobson Units (DU). One DU is equal to a column amount of 2.69×10^{16} molecules per cm^2 or about 0.01 mm of pure ozone at standard temperature and pressure. Equivalently, an ozone number density of 10^{12} molecules per cm^3 is equivalent to 3.7 DU per kilometer (km). The bottom panel is the vertical integral of the middle panel. The annual average flow field stream lines are shown in the top and middle panels. The rising motion in the tropical stratosphere and sinking motion in the polar region is known as the Brewer-Dobson circulation. Adapted from McPeters *et al.* (2007).

Ozone is destroyed when it reacts with oxides of nitrogen, hydrogen, chlorine, bromine, or oxygen atoms in catalytic reactions to reform molecular oxygen.

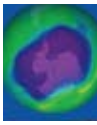

$$O_3 + X \rightarrow O_2 + XO \quad (2a)$$
$$XO + O \rightarrow O_2 + X \quad (2b)$$
$$O_3 + h\nu \rightarrow O_2 + O \quad (2c)$$
Net: $2\ O_3 + h\nu \rightarrow 3\ O_2$

The catalytic reactions that cause stratospheric ozone decreases are principally those involving chlorine and bromine.

Here, X represents the catalysts chlorine atoms (Cl), bromine atoms (Br), and the oxides of nitrogen (nitric oxide, NO) and hydrogen (hydroxyl, OH), while hν represents the absorption of solar ultraviolet light to photochemically break a chemical bond of ozone. The net effect of the catalytic cycle is to destroy two ozone molecules while regenerating the catalytic agent. All of these catalysts are highly reactive free radicals, meaning they have an unpaired electron, which tends to attach to other molecules in order to form a chemical bond. Since these reactions have an initial energy barrier to reaction, warmer temperatures will speed up this catalytic cycle, and cooler temperatures (as predicted to occur by recent climate models) will slow down this ozone loss cycle. In Figure 3.1, ozone decreases above 32 km as this ozone destruction begins to dominate over the ozone production.

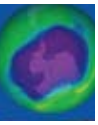

The source gases for the ozone-destroying catalysts are compounds such as chlorofluorocarbons, CFCs (chlorine), halons and methyl bromide (bromine), nitrous oxide (nitrogen), and methane (hydrogen) (see Chapter 2 for a complete discussion of these source gases). The relative contributions of the oxides of hydrogen (HO_x), oxides of chlorine (ClO_x), and oxides of nitrogen (NO_x) reactions can be found in Figure 1.11 of IPCC/TEAP (2005). As the air rises in the stratosphere, the catalytic agents are liberated from the source gases by both the UV radiation and chemical reactions.

The catalytic reactions that cause stratospheric ozone decreases are principally those involving chlorine and bromine. These chlorine and bromine compounds are from halogen species such as CFCs and halons. These species are inert in the troposphere, but are carried into the stratosphere by the slow rising circulation (Figure 3.1, top panel). As they ascend in the stratosphere, the halogen species are broken down by UV radiation or oxidation, releasing chlorine and bromine to catalytically destroy ozone. The rate of catalytic destruction of ozone is limited by the conversion of the chorine and bromine oxides to reservoir compounds such as hydrochloric acid (HCl), chlorine nitrate, ($ClONO_2$), and bromine nitrate ($BrONO_2$). These chlorine and bromine species are eventually returned to the troposphere, where they are removed in wet processes.

These ozone catalytic cycles involve oxygen atoms (O), and thus operate most rapidly in the mid-stratosphere of the tropics and the midlatitudes, where the concentration of oxygen atoms increases with increasing altitude. Oxygen atom concentrations increase with altitude because their loss slows as the density of O_2 and M ($O + O_2 + M \rightarrow O_3 + M$) decreases with altitude. Maximum halogen-catalyzed ozone loss at midlatitudes occurs around an altitude of about 40 km (just above the peak ozone concentrations), where these oxygen atoms are more abundant. While fractional ozone loss peaks near 40 km for a stratosphere unperturbed by cold temperatures (about 8 to 10% of the naturally-occurring ozone at that altitude), the contribution of ozone loss at 40km to the fractional loss in the total column is small, since ozone density falls off rapidly above the 20-25 km layer (Figure 3.1, middle panel).

Ozone depletion in the polar lower stratosphere involves different chemistry than described above. During winter, the lower stratosphere over the poles is characterized by air that the Brewer-Dobson circulation has carried poleward and downward from the upper stratosphere and mesosphere (Figure 3.1, top panel), extremely low temperatures (less than 200 K (−73°C)), and a circumpolar jet stream that isolates the air over the polar regions from midlatitude influence (the polar vortex). These extremely cold and isolated conditions enable polar stratospheric clouds (PSCs) to form (Crutzen and Arnold, 1986; Toon *et al.*, 1986). The ozone loss occurs in two steps. First, heterogeneous chemical reactions occur on the surfaces of the PSC particles, liberating chlorine from the two reservoir species ($HCl + ClONO_2$ [on PSCs]$\rightarrow$ $Cl_2 + HNO_3$) (Solomon *et al.*, 1986). Second, two principal chlorine and bromine catalytic reactions that do not involve oxygen reactions (Equation 1a) produce rapid depletion:

$$ClO + ClO + M \rightarrow ClOOCl + M \quad (3a)$$
$$ClOOCl + h\nu \rightarrow 2\ Cl + O_2 \quad (3b)$$
$$2\ [\ Cl + O_3 \rightarrow ClO + O_2\ ] \quad (3c)$$
Net: $2\ O_3 + h\nu \rightarrow 3\ O_2$

$$BrO + ClO + h\nu \rightarrow Br + Cl + O_2 \quad (4a)$$
$$Br + O_3 \rightarrow BrO + O_2 \quad (4b)$$
$$Cl + O_3 \rightarrow ClO + O_2 \quad \text{see (3c)}$$
Net: $2\ O_3 + h\nu \rightarrow 3\ O_2$

Equation (4a) represents a sequence of reactions that together lead to the products shown. Again, hν represents the absorption of solar light to photochemically break the chemical bonds, and M represents any air molecule, typically nitrogen (N_2) or oxygen (O_2), which carries away the excess energy of the reaction. In contrast to the intense UV necessary to photolyze oxygen molecules in (1a), the reactions (3b and 4a) require only visible light. These two catalytic cycles account for all but a few percent of the polar ozone loss, which occurs in the lowermost stratosphere (12 to 24 km altitude). This effect is strongest in the Antarctic stratosphere where the stable polar vortex allows the nearly complete destruction of ozone between about 12 and 22 km altitude each spring, forming the Antarctic ozone hole (see the low ozone amounts in Figure 3.1, bottom panel). The principal ingredients for large ozone losses in the polar regions are: (1) cold temperatures (< 195 K or −78°C) for the formation of PSCs; (2) high concentrations of chlorine and bromine; and (3) visible light for photolyzing both molecular chlorine (Cl_2) and the ClO dimer (ClOOCl).

The dramatic seasonal ozone losses occur over Antarctica during the Austral spring August-October period (with more than 50% of the total column ozone depleted) and to a smaller extent over the Arctic during the Boreal spring February-March period. The difference in hemispheres has to do with the contrast between the presence of polar stratospheric clouds and the timing of the break up of the polar vortex in the two polar regions. First, PSC extent is much greater in the Antarctic due to colder stratospheric temperatures than in the Arctic. Thus, molecules to participate in the two catalytic cycles involving chlorine and bromine atoms are much more abundant in the Antarctic. Second, the Arctic vortex breaks up and warms at an earlier time in spring than the Antarctic, shutting off the ozone loss.

In the midlatitudes, ozone destruction can take place locally or ozone-depleted air may be transported from polar regions. During periods following major volcanic eruptions, the sulfur injected into the stratosphere can lead to enhanced aerosols in the lower stratosphere. The surfaces of these aerosols promote the conversion of reservoir compounds of chlorine and bromine back to catalytically active oxides that increase ozone destruction.

The dramatic seasonal ozone losses occur over Antarctica during August to October and to a smaller extent over the Arctic in February and March.

The solar UV radiation that reaches the Earth's surface is strongly screened by ozone. The UV radiation important for biological processes is described by two bands, UVA (315 to 400 nanometers, nm) and UVB (280 to 315 nm). In a cloud-free atmosphere, both UVA and UVB are scattered by both molecules (Rayleigh scattering) and aerosols, while UVB is also significantly absorbed by ozone. Ozone absorption increases rapidly with decreasing wavelength, which is why there is little detectable radiation below 280 nm at the Earth's surface. For a given sun angle, the relationship of percent UV increase to percent ozone decrease is proportional to the ozone absorption. Human exposure to UV radiation has both negative (*e.g.*, skin cancer and eye cataracts) and positive (*e.g.*, Vitamin D production) effects. The negative effects of UV overexposure are the major reason for concern over stratospheric ozone decreases. In addition to changes in ozone, long-term changes in the amount of aerosols and cloud cover affect exposure at the surface to all UV wavelengths.

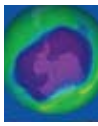

The following sections of this chapter briefly review the observed trends in ozone and ground ultraviolet radiation levels and discuss our current understanding of the processes that determine these levels. For each of these issues, the polar regions will be discussed separately from the low and midlatitudes because of the fundamentally different issues associated with those regions.

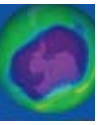

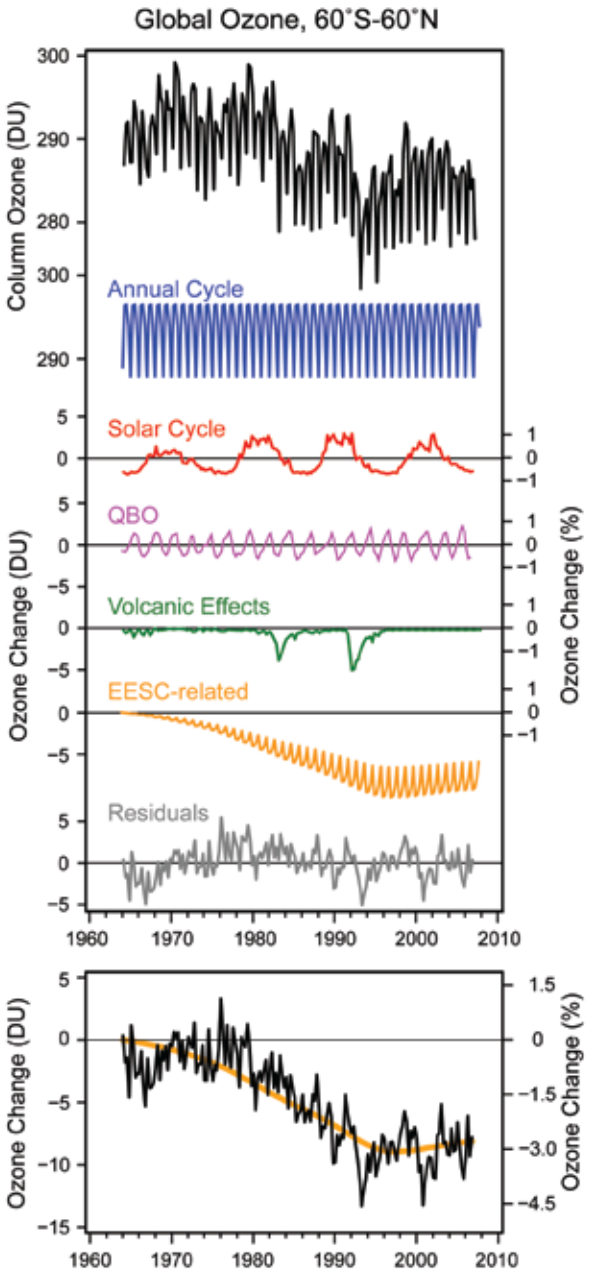

Figure 3.2 Top panel: Ozone observations for 60°S to 60°N estimated from ground-based data and individual components that comprise ozone variations (Dobson Units or DU). Bottom panel: Ozone deviations after removing annual cycle (blue line), solar cycle (red line), quasi-biennial oscillation or QBO (magenta line), and volcanic effects (green line) from original time series. Seasonal variations in the Equivalent Effective Stratospheric Chlorine (EESC) related component (up and down variations in orange line) are also removed. The thick orange line in the bottom panel represents the annual average EESC component derived from the regression model. See Box 3.1 for additional details.

3.2 OZONE

In this chapter we briefly review the most recent observed trends in observations of total ozone (Section 3.2.1) and ozone vertical distributions (Section 3.2.2). We then discuss our current understanding and recent findings related to the chemical and meteorological or dynamical processes that affect ozone (Section 3.2.3).

3.2.1 Total Ozone Observations

3.2.1.1 Global Ozone (Excluding Polar Regions)

After nearly two decades of decrease, the column amount of ozone at midlatitudes of the Northern and Southern Hemispheres has been relatively stable over the last decade. Polar ozone is considered in more detail in Section 3.2.1.3 below. We can integrate over the globe to get a simple measure of the recent changes in the ozone layer (Figure 3.2). The global mean total column ozone values for 2002-2005 were approximately 3% (about 10 Dobson Units or DU) below 1964-1980 average values. The 2002-2005 values are similar to the 1998-2001 values and this indicates that, overall, ozone is no longer decreasing. Several global datasets confirm this conclusion, although differences of up to 1% between annual averages exist between some individual sets (WMO, 2007).

Total column ozone over the tropics (25°S to 25°N) remains essentially unchanged. Total ozone trends in this region for the period 1980-2004 are not statistically significant, consistent with earlier assessments (Figure 3.4, WMO, 2007).

The behavior of ozone at midlatitudes in the Northern Hemisphere during the 1990s was different from that in the Southern Hemisphere during the same period. The Northern Hemisphere shows a minimum around 1993 resulting from forcings from the Mt. Pinatubo eruption and the solar cycle minimum, followed by an increase. The Southern Hemisphere shows an ongoing decrease through the late 1990s, followed by relatively constant levels (Figure 3.3). The average for the period 2002-2005 of total ozone at midlatitudes in each hemisphere is similar to the average for the previous four years, 1998-2001. Ozone in the southern midlatitudes remains about 5.5% below its 1964-1980 average, while ozone in the northern midlatitudes remains about 3% below (Figure 3.3).

BOX 3.1: Estimating Ozone Trends

Isolating the ozone response to manmade ozone-depleting substances from natural variations in the ozone, such as seasonal changes or volcanic perturbations, is accomplished using a statistical time series regression analysis. The top panel of Figure 3.2 (black line) shows total ozone time series from ground-based measurements taken over the period 1964 to 2006 and averaged seasonally and over the 60°N-60°S area (87% of the Earth's area). The observations are statistically modeled as a linear combination of the known individual processes that cause ozone to vary. In this analysis (following Fioletov *et al.*, 2002), the regression model used is:

$$O_3(t) = \mu + \text{seasonal cycle} + \alpha \cdot EESC + \beta \cdot QBO + \gamma \cdot Solar + \delta \cdot Volcano + noise$$

Here, μ, α, β, γ, and δ are constants estimated such that the model (terms on the right hand side) best matches the observed ozone time series. The mean (μ) and seasonal cycle are calculated directly from the ozone data from 1979 to 1987 (blue line in Figure 3.2). Equivalent Effective Stratospheric Chlorine (EESC, see Chapter 5) is used to represent anthropogenic trace gases that react with ozone (orange line in Figure 3.2). The magenta line shows the quasi-biennial oscillation (QBO). The QBO is a variation in stratospheric winds with a period of about 26 months that is represented using equatorial radiosonde wind observations (Reed *et al.*, 1961). The solar term is represented using the 10.7 cm radio flux measured at Ottawa, Canada (red line). The volcanic term is derived from stratospheric aerosol observations (dark green). The noise term includes all variations required to make the model exactly equal the observed ozone (grey). The coefficients (μ, α, β, γ, and δ) are estimated by a mathematical regression that minimizes the noise term.

The bottom panel highlights the ozone changes due to chlorine and bromine (*i.e.*, EESC) with the natural forcings (seasonal cycle, QBO, solar, and volcano) removed. This line is the original observations with only the annually-averaged EESC-related time series (smoothed orange line) and the residual noise term remaining (grey line).

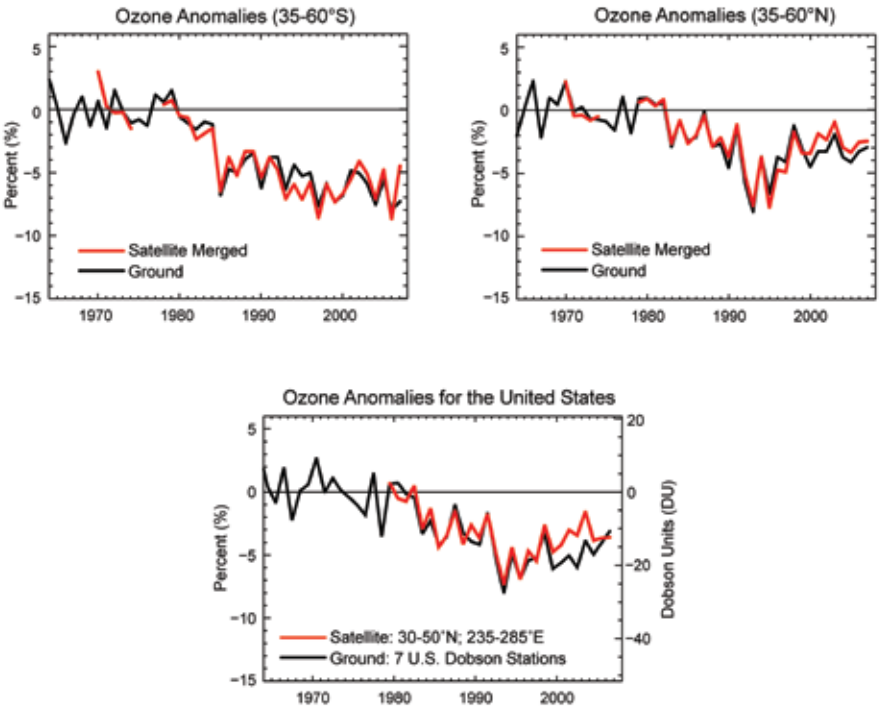

Figure 3.3 Top: deseasonalized, annually averaged, area-weighted total ozone deviations from satellite (red) and ground stations (black) for the latitude bands 35°N to 60°N (left) and 35°S to 60°S (right). Anomalies were calculated with respect to the time average for the period 1964-1980. Updated from Fioletov *et al.* (2002) and WMO (2003). Bottom: Average total ozone over the United States from the TOMS/SBUV series of satellite instruments (red), and seven ground stations in the United States. Both time series are plotted relative to the 1964-1980 mean of the ground-station data. Updated from Stolarski and Frith (2006).

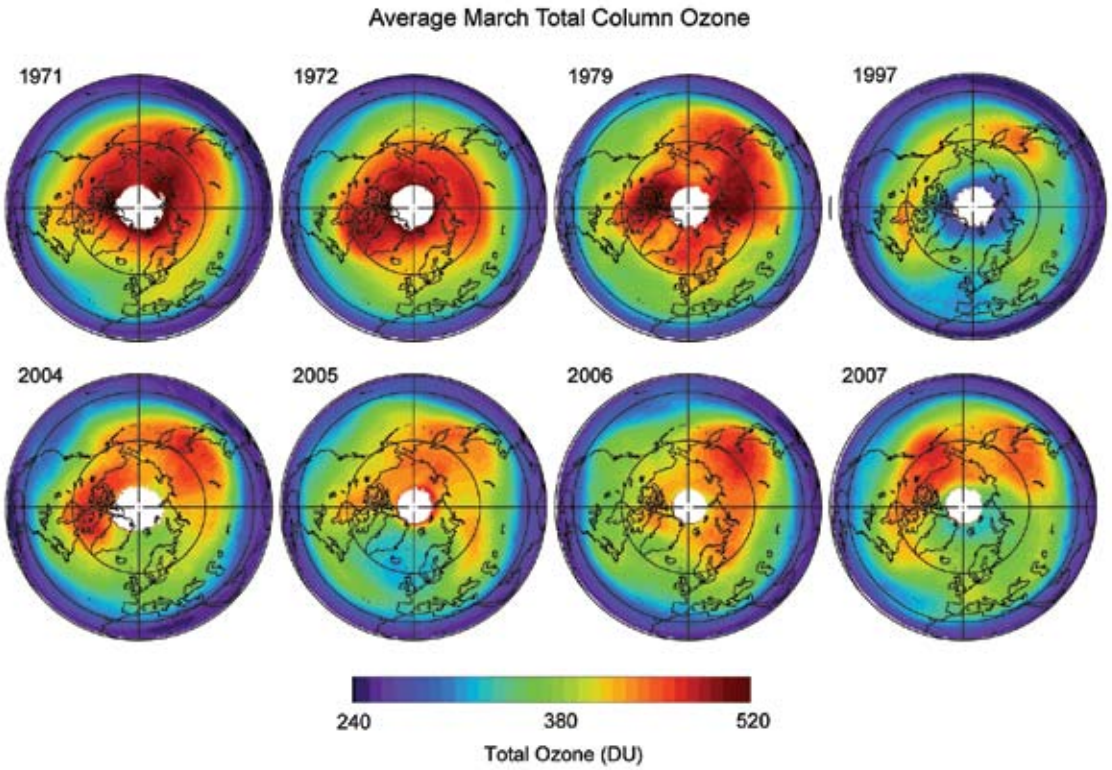

Figure 3.4 March monthly averaged total ozone. The 1971 and 1972 images are from the Nimbus-4 BUV instrument, the 1979 is from the Nimbus-7 TOMS satellite instrument, the 1997 and 2004 images are from the Earth Probe TOMS, and the 2005, 2006, and 2007 images are from the Aura Ozone Monitoring Instrument (OMI). This figure is updated from Figure 4-6 of WMO (2007).

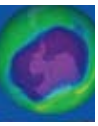

Releases of ozone-depleting substances in the United States affect global ozone levels, and releases across the globe affect the United States, because of the long lifetimes of CFCs and their mixing, or spread, around the world.

Total ozone over the United States tends to parallel the entire Northern Hemisphere because these levels are driven by the response to the worldwide chlorine and bromine releases and by hemispheric-scale transport processes (Figure 3.3, bottom). Releases of ozone-depleting substances in the United States affect global ozone levels, and releases across the globe affect the United States, because of the long lifetimes of CFCs and their mixing, or spread, around the world. Total ozone over the United States is shown in the bottom panel of Figure 3.3. The total ozone changes are similar to ozone over the entire northern midlatitudes (compare to top right panel). The minimum value was reached shortly after the eruption of Mount Pinatubo and was about 5 to 8 percent below the amounts present prior to 1980 (as a result of the volcanic aerosol effect). The ozone increase since 1993 has diminished the ozone deficit to about 2 to 5 percent below the pre-1980 amounts. The average for the last four years (2002-2005) is essentially the same as the previous four years.

3.2.1.2 Polar Ozone

Significant ozone depletion has occurred in the polar regions over the last few decades as a result of anthropogenic halogen-containing compounds. The ozone loss chemistry, as described in Chapter 1 (also WMO, 2007 and references therein), begins with very cold temperatures that lead to the formation of PSCs. Chlorine is rapidly converted from inactive to reactive forms on the cold aerosol surfaces. The Antarctic ozone hole is the most extreme manifestation of this phenomenon. Reactive chlorine is released within the stratospheric polar vortex beginning in the winter darkness. In August through September, when sunlight has returned to the Antarctic, halogen photochemistry rapidly destroys ozone. Some ozone loss is also observed in the June-August period at the edge of the polar vortex (Roscoe *et al.*, 1997). Ozone loss maximizes by the late September to early October period, after which temperatures warm, ozone loss ceases, the polar vortex breaks up, and high ozone air from midlatitudes mixes in, rapidly filling in the ozone hole (typically in the November-December period).

In this section, we illustrate trends in total ozone for both the Arctic and Antarctic. The ozone content in the polar lower stratosphere is dependent on background chemical conditions, temperatures, transport, and dynamics. The Arctic polar stratosphere shows large interannual variability, while the Antarctic is more stable because the Antarctic polar vortex is more stable. This section discusses the behavior of polar ozone over the last few decades. Section 3.2.1.2.1 focuses on the Arctic, while 3.2.1.2.2 shows the Antarctic.

3.2.1.2.1 Arctic total ozone

Arctic total ozone has had a substantial downward trend since the 1970s with slightly higher values over the last ten years than in the previous six years. Figure 3.4 displays a series of March polar averages for selected years from 1971 to 2007 (updated from Figure 4-6 in WMO, 2007). The 60°N latitude circle generally encloses the region of ozone depletion, but in some years (*e.g.*, 2005) the vortex and low ozone region are displaced from the pole, extending somewhat southward of 60°N. Nevertheless, Arctic ozone for recent March averages is low compared to the observations prior to 1980 (shown in the upper row of Figure 3.4).

The springtime average total ozone values in the Arctic poleward of 63°N latitude (upper line) are shown in Figure 3.5, in comparison with the average total ozone for the years 1970-1982 (gray horizontal line). The difference between the observed values and the 1970-1982 average indicates the combined changes in ozone due to chemistry and dynamics. In the last ten years Arctic column ozone is higher than the low values of the mid-1990s, except in the cold and chemically active winter of 1999/2000, when a large decrease of 63°-90° Northern Hemispheric total ozone was observed (Rex *et al.*, 2002).

The record-cold winter of 2004/2005 led to very large ozone losses (Manney *et al.*, 2006; Rex *et al.*, 2006; Singleton *et al.*, 2007; Goutail *et al.*, 2005; Feng *et al.*, 2007a). However, this large loss showed a less pronounced impact on the March polar average total ozone. Although Northern Hemisphere polar column ozone averages are a general indicator of Arctic ozone depletion and trends (WMO, 2007), the chemical loss can oftentimes be masked by the 63-90°N polar averaging. For example, the 2005 March average had a strong influence of dynamics. Vortex fragments moved outside the 63°-90°N and the total ozone showed a distinct minimum near 60°N (Figure 3.4). This created a higher value relative to other recent cold winters even though chemical ozone loss in the lower stratospheric vortex in mid winter of 2005 was as high as or higher than ozone loss in other recent cold winters.

Arctic total ozone has had a substantial downward trend since the 1970s, with slightly higher values over the last ten years than in the previous six years.

3.2.1.2.2 Antarctic total ozone

In the Southern Hemispheric (SH) polar region, very large ozone depletions in the Austral spring have led to extremely low ozone values over Antarctica during October, the "ozone hole" (Figure 3.5, bottom line). Figure 3.6 displays a series of Antarctic total ozone images (values shown in Figure 3.5 are averaged from these images). A comparison of the moderate values of total ozone over

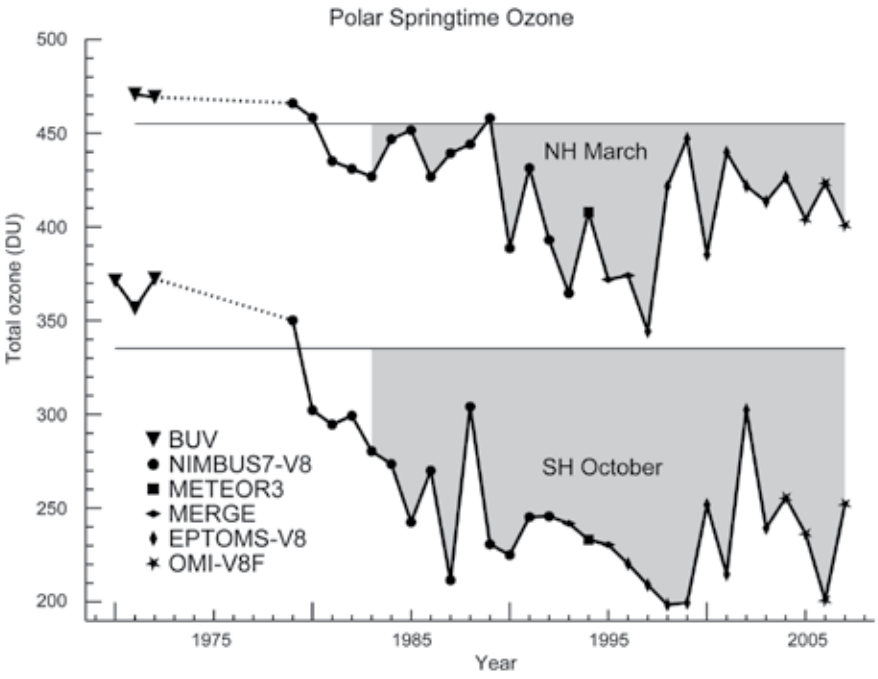

Figure 3.5 Total ozone average of 63°-90° latitude in March (Northern Hemisphere) and October (Southern Hemisphere). Symbols indicate the satellite data that have been used in different years. The horizontal gray lines represent the average total ozone for the years prior to 1983 for the Northern Hemisphere and Southern Hemisphere. The grey shading shows the contribution of chemical ozone destruction and natural variations. Updated from Figure 4-7, WMO (2007).

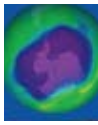

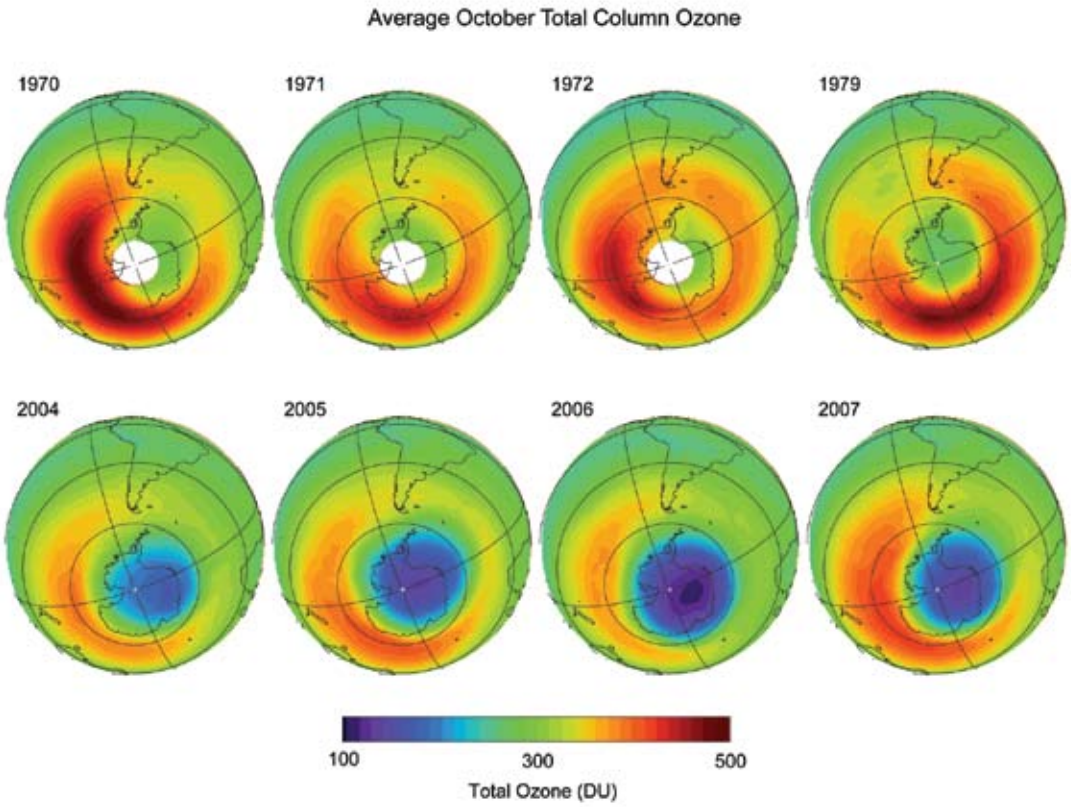

Figure 3.6 Satellite observations of October monthly averaged total ozone. The 1970, 1971, and 1972 images is from the Nimbus-4 BUV instrument, the 1979 image is from the Nimbus-7 TOMS instrument, and the 2004, 2005, 2006 and 2007 images are from the Aura OMI instrument.

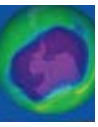

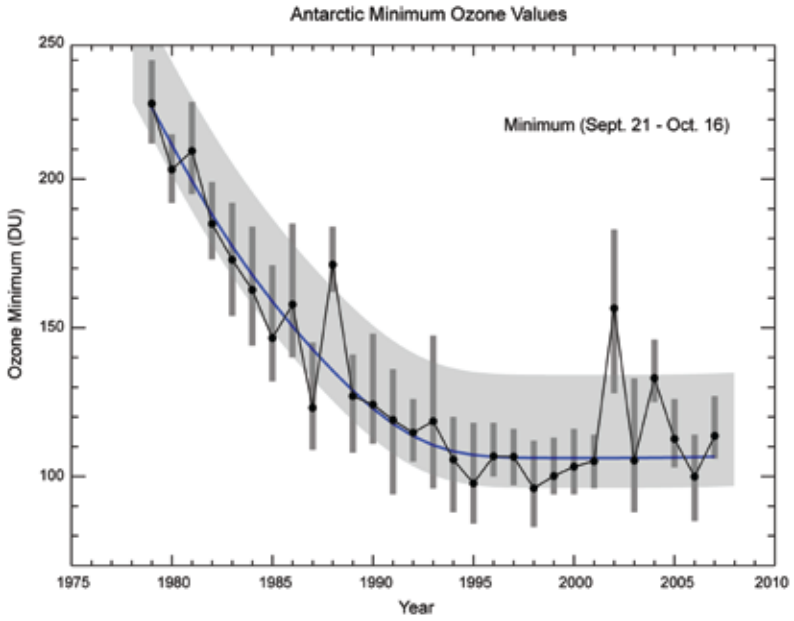

Figure 3.7 The minimum ozone values over Antarctica are averaged for the period from 21 September to 16 October (black dots). The vertical grey bars indicate the range of ozone values used in the average. The blue line shows the fit to these ozone values as was shown in Newman *et al.* (2004), and now using EESC, as derived in Newman *et al.* (2006) (also Box 2.7 in Chapter 2). The EESC has a mean age of 5.5 years, an age spectrum width of 2.75 years, and a bromine-scaling factor of 60. The fit is quadratic in EESC. The background lighter grey shading shows the expected variation of minimum ozone values between warm (upper side = +10°C) and cold years (lower side = −10°C). This figure was generated using TOMS and OMI total ozone. Updated from Figure 4-8 of WMO (2007).

Antarctica in the early years (1970s, top row) to the reduced values over Antarctica in the last two decades (bottom row) illustrates the Antarctic ozone hole. In Figure 3.5, the years from 2000 to 2005 showed an increase in polar column ozone averages compared to 1998 and 1999. The interannual variations in ozone depletion observed from 2001 to 2005 primarily result from variations in the dynamics (*i.e.*, stratospheric weather variations), and have not been caused by changes in Equivalent Effective Stratospheric Chlorine (EESC). See Box 2.7 of Chapter 2 for a definition of EESC and see Chapter 5 for more discussion on its usage. Since the early 1990s, total loss of ozone occurs in the lowermost stratosphere inside the polar vortex in September and October (Solomon *et al.*, 2005). Estimates of EESC inside the vortex reached a value of about 3.2 parts per billion by mole (ppb) in 1990 and peaked in early 2001 at about 4.0 ppb (Newman *et al.*, 2007). Hence, the EESC concentrations since the early 1990s have exceeded those necessary to cause total loss. The Antarctic ozone hole, therefore, has had low sensitivity to moderate decreases in EESC and the unusually small ozone holes in some recent years (*e.g.*, 2002 and 2004) are strongly

attributable to a dynamically driven warmer Antarctic stratosphere.

Various metrics that capture different aspects of the Antarctic ozone hole are used to describe the severity of ozone depletion, such as Antarctic ozone hole area, ozone minimum, ozone mass deficit, and profile shape (Section 3.2.2.2). The polar average from 63-90°S tends to exaggerate dynamical fluctuations (Figure 3.5). Figure 3.7 displays the Antarctic ozone hole minimum values averaged for the period 21 September to 16 October. Because the Antarctic ozone hole chemical losses peak in late September, the average minimum ozone columns in this period provide a very useful metric for the depletion severity. Again, this figure shows a clear decrease from 1979 to the mid-1990s, with particularly low values in the mid- to late 1990s. Following Newman *et al.* (2006), we have added a statistical fit of these metrics (blue line) to a quadratic function of Antarctic EESC. The fit shows how ozone levels have responded to chlorine. In addition to the fit to chlorine, the figure also includes a background grey shading that shows the expected natural variation of the ozone minimum values for warmer than average years ($+2\sigma = 10$ K, upper part) and colder years ($-2\sigma = -10$ K, lower part). The 2002 minimum value stands out because it was the warmest year on record. The minimum ozone values in 2002 and 2004 were higher than the expected values (the blue line) because of the warmer temperatures.

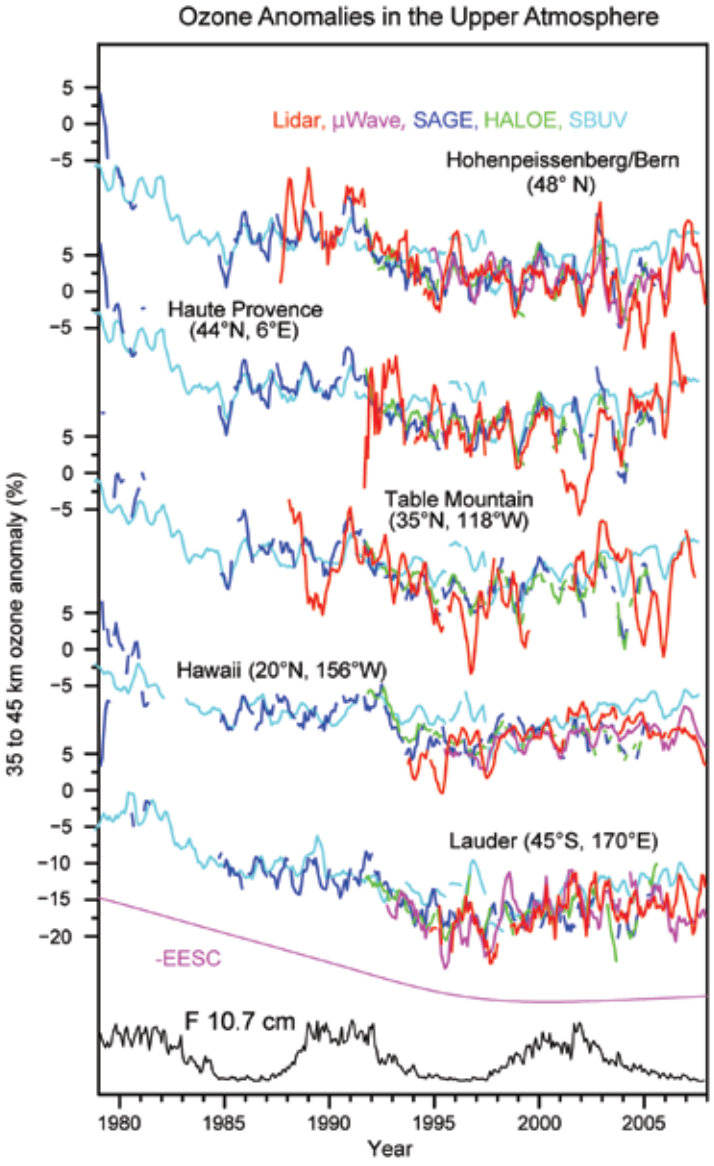

Figure 3.8 Time series of upper stratospheric ozone anomalies measured by ground-based lidar and microwave radiometers at five stations and corresponding zonal means from satellite (SAGE, HALOE, and SBUV) measurements (updated from Steinbrecht *et al.*, 2006 and WMO, 2007).

3.2.2 Vertical Distribution of Ozone

3.2.2.1 Global

In addition to the polar regions, the upper stratosphere also shows clear evidence for ozone destruction due to increasing chlorine compounds. Measurements from both the Stratospheric Aerosol and Gas Experiment (SAGE I+II) and Solar Backscatter Ultraviolet (SBUV[/2]) satellite instruments show significant declines in upper stratospheric ozone from 1979 through 2004 (Figure 3.8). The net ozone decrease over the 1979 to 1995 period was approximately 10-15% over midlatitudes, with smaller but significant changes over the tropics (Figure 3-7 in WMO, 2007). During the last decade, upper stratospheric ozone has remained relatively constant. Available independent Umkehr ground-based optical remote sensing, Light Detection and Ranging (lidar) remote sensing, and microwave ozone measurements confirm these findings.

The bulk of column ozone is found in the lower part of the stratosphere (Figure 3.1). The evidence shows that lower stratospheric ozone declined over the period 1979-1995, but has been relatively constant with significant variability over the last decade. Figure 3.9 shows the vertical profile of ozone trends in midlatitudes of the Northern (left panel) and Southern (right panel) Hemispheres. The trends are actually fits to EESC ($\Delta O_3 = \alpha \bullet \Delta EESC$, see Box 3.1) that is converted to a percentage per

The Antarctic ozone hole first began to develop in the early 1980s and reached its current full extent by the mid-1990s.

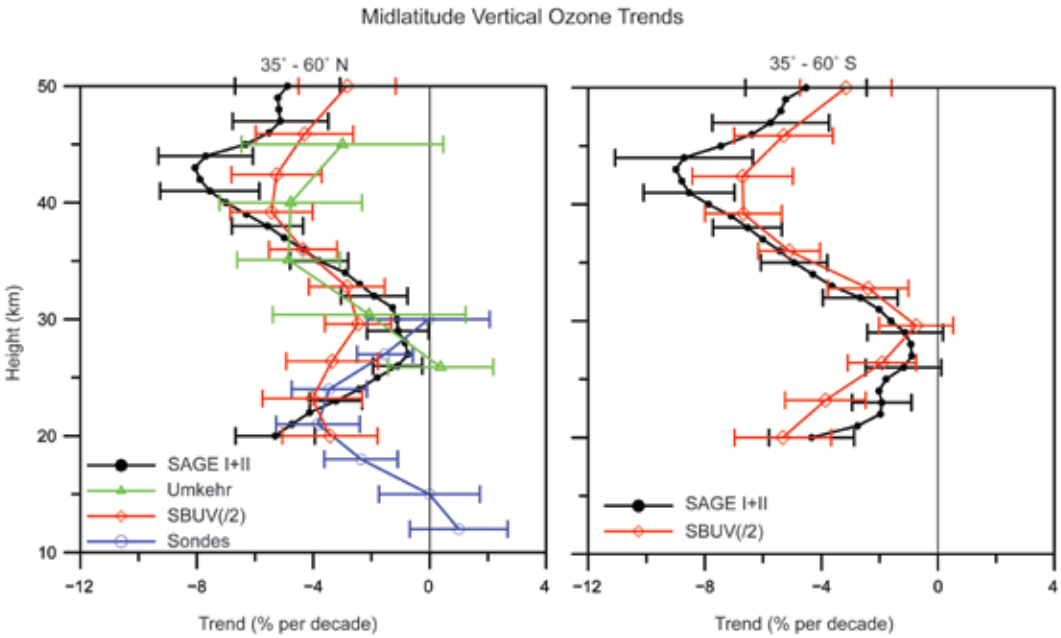

Figure 3.9 Vertical profile of ozone trends over northern and southern midlatitudes estimated from ozonesondes, Umkehr, SAGE I+II, and SBUV(/2) for the period 1979-2004. The trends were estimated using regression to an EESC curve and converted to % per decade using the variation of EESC with time in the 1980s. The trends were calculated in geometric altitude coordinates for SAGE and in pressure coordinates for SBUV(/2), sondes, and Umkehr data, and then converted to altitude coordinates using the standard atmosphere. The two standard deviation error bars are shown.

decade by scaling the α coefficient with the linear 1 ppb change of EESC observed during the 1980s. Measurements by SAGE I+II and SBUV(/2) showed declines of 7 to 9% (or 10 to 15% cumulative by 1995) between 40 and 45 km altitude (Figure 3.9).

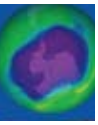

These midlatitude ozone decreases are not linear, and did not continue in the last decade. This non-linear trend has been accounted for by using the ozone regression against the EESC time series and then converting to % per decade using the variation of EESC with time in the 1980s. At lower altitudes, between 12 and 15 km, in the Northern Hemisphere, a strong decrease in ozone was observed from ozonesonde data between 1979 and 1995, followed by an overall increase from 1996 to 2004, leading to no net long-term decrease at this level. These changes in the lowermost stratosphere have a substantial influence on the column because most of the ozone resides in the lowermost stratosphere.

3.2.2.2 Polar

The Antarctic ozone hole first began to develop in the early 1980s and reached its current full extent by the mid-1990s (Hofmann *et al.*, 1997; Solomon *et al.*, 2005). The most complete record of the morphology of the Antarctic ozone hole vertical structure is found from the balloon-borne ozonesonde

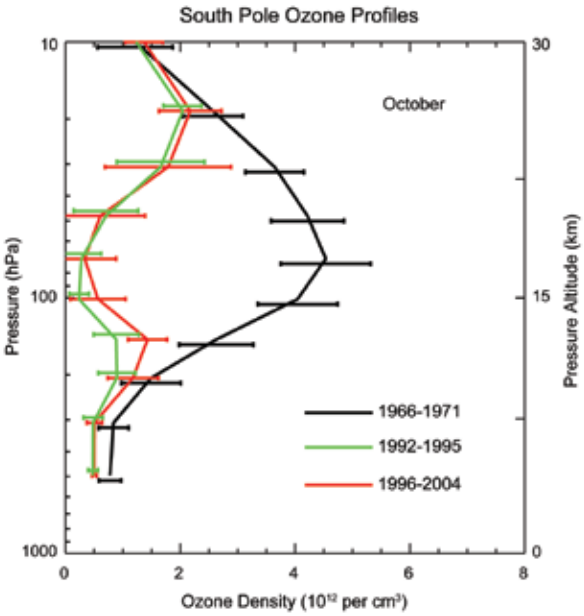

Figure 3.10 Observations of the October average ozone profiles measured at the South Pole in different time periods; prior to the Antarctic ozone hole (1966-1971), after the Mt. Pinatubo eruption when aerosol abundances were enhanced in (1992-1995), and current conditions (1996-2004). Adapted from Solomon *et al.* (2005).

measurements at the South Pole, which extend back to the mid-1960s. Figure 3.10, from Solomon *et al.* (2005), uses the South Pole ozonesonde data to delineate the Antarctic ozone hole region relative to the pre-ozone hole conditions of the 1970s. The altitude range of the Antarctic ozone hole has been very stable in the 1990s. In the vicinity of the lower edge of the Antarctic ozone hole (10 to 14 km), Figure 3.10 shows that ozone abundances were lowest in the 1992-95 time period. This is presumably the result of increased ozone loss resulting from the enhanced aerosol loading after the Mt. Pinatubo eruption (Hofmann *et al.*, 1997; Solomon *et al.*, 2005).

Also of interest is the ozone variability near the top edge of the Antarctic ozone hole. Ozone abundances in this layer between 18 and 22 km may provide an early indication of Antarctic ozone hole recovery (Hofmann *et al.*, 1997). However, as discussed further below, the higher abundances in the 2001-2004 period have been attributed to meteorological variations rather than to ozone recovery (*e.g.*, Hoppel *et al.*, 2005). During 2002-2004, the temperature in the 20-22 km region tended to be warmer than average from mid-August through September, resulting in fewer PSCs which inhibited ozone loss (Hoppel *et al.*, 2005). The most extreme manifestation of this inhibited ozone loss occurred in 2002. As described in Section 3.2.3.1.1, in September of that year the first documented Antarctic major warming event took place (Roscoe *et al.*, 2005). Major warmings are defined as reversals of both the vortex flow and the temperature gradient in the middle stratosphere; these events are relatively common in the Arctic, but had not been previously observed in the Antarctic. In 2002, anomalously high ozone levels and temperatures extended down to 15 km.

The Antarctic ozone hole generally behaves in a regular fashion, since the Antarctic winter stratosphere is consistently cold, with a stable, isolated vortex and an abundance of PSCs each winter. As discussed in Section 3.2.3.1.1, the Arctic winter stratosphere exhibits much more variability. Compared to the Antarctic, the Arctic is generally warmer with fewer PSCs (Fromm *et al.*, 2003 Figure 3-13). Periods of cold temperatures with elevated reactive chlorine also tend to persist for shorter lengths of time in the Arctic and these cold regions are generally not concentric with the Arctic polar vortex, but are frequently centered roughly in the region between Greenland and Norway. Thus, ozone levels in the Arctic lower stratosphere exhibit a large amount of variability, which is well correlated with temperature. This is primarily the result of the fact that in the Arctic lower stratosphere the average temperature is very near the PSC formation threshold temperature. Therefore, in cold winters, PSCs tend to be very abundant and large halogen-catalyzed ozone depletion occurs, whereas in warm winters PSCs are very infrequent and little chemical ozone depletion occurs (Rex *et al.*, 2004). This is illustrated later in Section 3.2.3.1.1 in Figure 3.12, which shows a very good correlation between the volume of air with temperatures cold enough to be capable of forming PSCs and the chemical loss of ozone in the lower stratosphere.

Compared to the Antarctic, the Arctic is generally warmer with fewer polar stratospheric clouds (PSCs), which play a role in the depletion of the ozone layer.

A particular problem with regard to assessing trends in polar ozone loss is that the distribution and variation of stratospheric ozone are controlled by both transport processes and photochemical processes. Ozone trends resulting from changes in atmospheric halogen loading must be separated from trends resulting

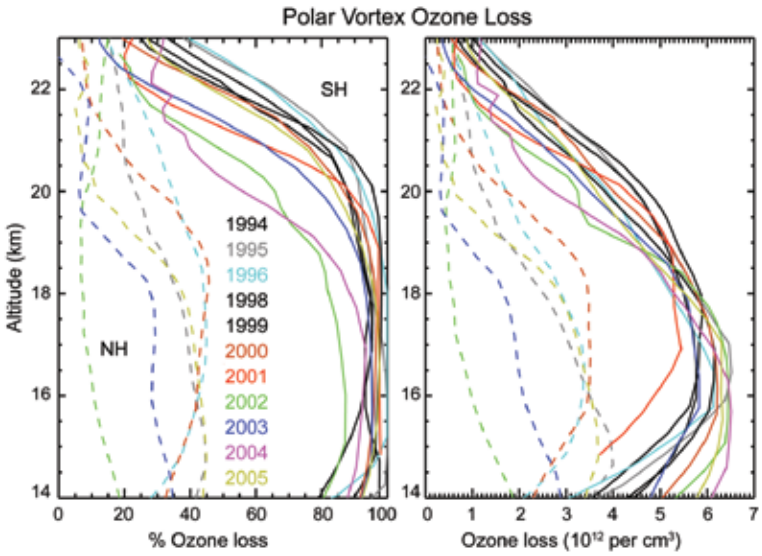

Figure 3.11 Ozone loss estimates from the Polar Ozone and Aerosol Measurement (POAM II & III). Southern Hemisphere October 5 estimates (solid lines) and Northern Hemisphere March 10 estimates (dashed lines) are based on the "vortex average technique" described in WMO (2007) and Hoppel *et al.* (2002, 2003). Estimates are shown only for Northern Hemisphere winters which had a relatively persistent, isolated vortex from January 1 - March 10.

from transport variations. Instruments measure ozone abundances and their variations, but do not directly measure ozone photochemical loss. Isolating the photochemical ozone change in the Arctic is more complicated than in the Antarctic because of the much larger degree of dynamical variability. Several different methods have been developed for isolating photochemically driven ozone change from transport-driven change. For cold Arctic winters (in which there is measurable loss), ozone loss derived from each of these methods now agree fairly well (*e.g.*, WMO, 2007, Figure 4-11). Therefore, we now have a fairly reliable record of ozone chemical loss for all Antarctic winters, and for cold Arctic winters, dating back to the mid-1990s. As an example, Figure 3.11 shows vertical profiles of photochemical loss derived from Polar Ozone Aerosol and Measurement (POAM II & III) measurements, for both the Arctic and Antarctic, during the 1994-2005 time period (Hoppel *et al.*, 2003). Ozone loss in the Antarctic ozone hole was fairly stable in the 1990s, with nearly complete loss in the 14 to 19 km altitude range. Figure 3.11 shows that the anomalously high ozone levels in the upper region of the Antarctic ozone hole in 2001 through 2004 were the result of reduced ozone chemical loss. In contrast to the Antarctic, the ozone loss profiles for the Arctic are highly variable with peak losses of almost 50% (losses up to approximately 60% have been reported by other analyses [Rex *et al.*, 2004; WMO, 2003; WMO, 2007]).

The Antarctic ozone hole is more severe in colder than average years, while less severe in warmer than average years.

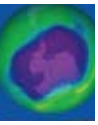

3.2.3 Processes That Affect Ozone

3.2.3.1 Transport and Dynamics

Stratospheric ozone levels are strongly influenced by both transport and the temperatures of the stratosphere. In this section, we will summarize the influence of dynamical processes on ozone levels. First, there is the direct influence of winds that carry ozone-enriched air from the photochemical production region into other regions, thereby increasing ozone. Second, the opposite process can occur where winds carry ozone-depleted air into other regions, thereby decreasing ozone (*e.g.*, from the Antarctic ozone hole into the midlatitude stratosphere). Third, the radiatively and dynamically driven local temperature can influence ozone by affecting catalytic loss reaction rates.

This section is divided into two subsections. The first subsection discusses the influence of dynamics on polar ozone, while the second subsection addresses the influence of dynamics on midlatitude ozone.

3.2.3.1.1 Polar

Variability in the dynamical conditions in the troposphere/stratosphere system results in variability of ozone transport and temperatures in the polar stratosphere. Previous World Meteorological Organization (WMO)/ United Nations Environment Programme (UNEP) assessments have shown that, on short timescales, interannual variability in polar ozone chemistry is mainly driven by temperature variability, which in turn is the result of variable dynamical conditions. The combined effect of dynamically-induced variability in both chemistry and transport is the main driver of interannual variability of the abundance of ozone in the polar stratosphere.

As described in the Introduction (Section 3.1), the air in the polar lower stratosphere is transported downward from the upper stratosphere and mesosphere over the course of the winter period by the Brewer-Dobson circulation. The Brewer-Dobson circulation is driven by large-scale atmospheric waves that propagate upward from the troposphere. Figure 3.1 shows this poleward and downward circulation in the annual average. This upper stratospheric air has on average been in the stratosphere for five to six years since entering the stratosphere at the tropical tropopause. In the absence of polar ozone destruction, this air would be characterized by relatively high ozone concentrations. Furthermore, because the air has been in the upper stratosphere and exposed to intense solar UV, the organic chlorine and bromine compounds have been almost completely converted to inorganic forms that can participate in ozone loss processes.

The chemical ozone loss processes precipitated by the presence of halogens are initiated by the formation of PSCs in the extremely cold polar lower stratosphere (Crutzen and Arnold, 1986; Toon *et al.*, 1986). PSCs provide a surface upon which heterogeneous (not gas-phase, but at the surface between a solid/liquid and a gas) reactions take place that convert comparatively

unreactive chlorine reservoirs into ones that are exceedingly reactive in sunlight. While the chlorine and bromine levels in the stratosphere directly cause ozone loss, year-to-year variation of the chemically driven polar ozone loss is directly tied to the temperature by a modulation of polar stratospheric clouds and transport.

A number of studies have shown that the Antarctic ozone hole is more severe in colder than average years, while less severe in warmer than average years (Newman and Randel, 1988; WMO, 1989). In the Arctic, Rex *et al.* (2004) quantitatively related the volume of polar stratospheric clouds (V_{PSC}) to the chemical ozone loss estimated from ozonesondes (extended to the Antarctic by Tilmes *et al.*, 2006). Figure 3.12 shows ozone loss plotted against V_{PSC} for the years from 1992 to the present (the latest data are available through 2007). This 1992-2007 period has high chlorine and bromine levels (Chapter 2). For the coldest Arctic winters, the volume of air with temperatures low enough to support polar stratospheric clouds (V_{PSC}) increased significantly since the late 1960s (Rex *et al.*, 2006). The cooling of the lower stratosphere is much larger than expected from the direct radiative effect of increasing greenhouse gas concentrations. The reason for the change is not clear and it could be due to long-term natural variability or an unknown dynamical mechanism.

The year-to-year variation of spring temperatures in the polar stratosphere is primarily driven by year-to-year variability of planetary waves that propagate upward from the troposphere to the stratosphere. The relationship of waves to stratospheric ozone was recognized by a number of early investigators who saw large increases of total ozone following major stratospheric warmings (London, 1963).

The large variability of polar total ozone shown in Figures 3.5 and 3.7 is directly tied to the variations in the levels of the planetary waves (Randel *et al.*, 2002). The Southern Hemisphere winter of 2002 provides an excellent example of a year with extremely high levels of planetary waves propagating into the stratosphere. The planetary wave forcing of the stratosphere is estimated from the eddy heat flux (a cross correlation of the north-south wind and the temperature) at an altitude of 16 km in the 45-75°S zone (see Andrews *et al.* (1987) for a more complete description of the wave driving of the stratosphere by the troposphere). In September 2002, a major warming had a dramatic impact on total ozone, splitting the Antarctic ozone hole into two pieces (Stolarski *et al.*, 2005). Meteorological conditions in 2002 showed that the early winter was already unusually disturbed (Hio and Yoden, 2005; Newman and Nash, 2005; Allen *et al.*, 2003). There were several significant wave events from May to October that each warmed the stratosphere by a few degrees until the major warming in late September. Several models reproduced the chemistry and dynamics of this 2002 warming, revealing the direct impact of tropospheric waves on Antarctic ozone levels (Manney *et al.*, 2005; Ricaud *et al.*, 2005; Konopka *et al.*, 2005; Grooß *et al.*, 2005; Sinnhuber *et al.*, 2003; Feng *et al.*, 2005).

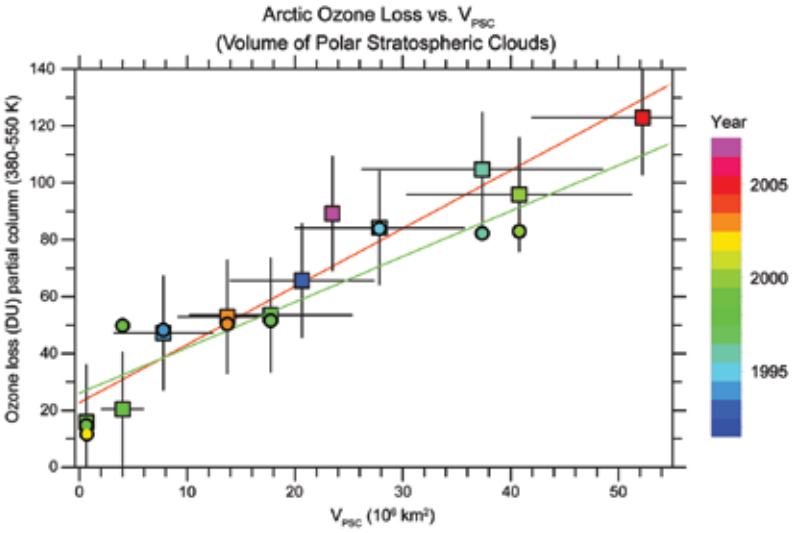

Figure 3.12 Scatter plot of vortex-average chemical loss of column ozone (ΔO_3, calculated over the range 380 to 550 K) versus V_{PSC} inferred from ozonesonde observations for the 1991/1992 to 2006/2007 Arctic winters (update from Rex *et al.*, 2004). Colored squares and the red fit line show results based on ozonesonde analyses; colored circles and the green fit line show results from tracer correlation studies based on HALOE data (update from Tilmes *et al.*, 2006). Adapted from Rex *et al.* (2006, 2004), and Tilmes *et al.* (2006).

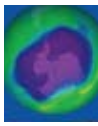

The lifetime of ozone in the midlatitude lower stratosphere (16 to 30 km) is more than 100 days. Therefore, transport through the atmosphere plays a very important role in determining midlatitude ozone levels.

3.2.3.1.2 Midlatitude dynamic and transport effects on ozone

The influence of transport and dynamics on the midlatitude lower stratosphere (16 to 30 km) and lowestmost stratosphere (8 to 16 km) principally occurs through the Brewer-Dobson circulation and through mixing processes. While photochemistry plays an important role

Heterogeneous reactions on polar stratospheric clouds (PSCs) convert the comparitively unreactive chlorine reservoirs into chlorine that is very reactive in sunlight.

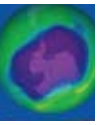

for ozone in the midlatitudes, the lifetime of ozone in the lower stratosphere is long (greater than 100 days), and hence, transport plays a very important role in determining ozone levels. In the upper stratosphere, dynamically or radiatively forced temperature changes can have a large effect on ozone loss rates by modifying the catalytic loss processes. Dynamically forced ozone changes in the lower stratosphere occur because of:

- interannual and long-term changes in the strength of the stratospheric Brewer-Dobson circulation (Figure 3.1), which is responsible for the winter-spring buildup of extratropical ozone (*e.g.*, Fusco and Salby, 1999; Randel *et al.*, 2002; Weber *et al.*, 2003; Salby and Callaghan, 2004a; Hood and Soukharev, 2005) and;
- changes in tropospheric circulation, particularly changes in the frequency of local nonlinear synoptic wave forcing events, which lead to the formation of extreme ozone minima ("mini-holes") and associated large increases in tropopause height and horizontal mixing (Steinbrecht *et al.*, 1998; Hood *et al.*, 1997, 1999, 2001; Reid *et al.*, 2000; Orsolini and Limpasuvan, 2001; Brönnimann and Hood, 2003; Hood and Soukharev, 2005; Koch *et al.*, 2005).

The effects of dynamics on ozone trends and variability are extremely difficult to quantify. This difficulty is caused by the relationship between the strength of the Brewer-Dobson circulation, the wave mixing processes, and the position and strength of the polar vortex. As is well recognized, the propagation of planetary scale waves from the troposphere into the stratosphere drives the Brewer-Dobson circulation, while at the same time the breaking of these waves irreversibly mixes air latitudinally. The estimation of ozone advection is further confused by the need to multiply the transport "variables" by the ozone horizontal and vertical gradients. This effect of the ozone gradient is mainly evident in two regions: the mixing of lower stratospheric ozone depleted air from the polar latitudes to the midlatitudes during the spring period, and the mixing of air from the tropical upper troposphere (with very low ozone amounts) into the midlatitude lowermost stratosphere.

Empirical studies using inferred circulation changes indicate that a substantial fraction of the observed Southern Hemisphere and Northern Hemisphere variability results from variations of the wave driving and by inference the Brewer-Dobson circulation (Salby and Callaghan, 2002; Salby and Callaghan, 2004a; Salby and Callaghan, 2004b; Randel *et al.*, 2002; Hood and Soukharev, 2005). Randel *et al.* (2002) and Hood and Soukharev (2005) estimated that 18-30% of the spring column ozone trends from 1979 to the mid-1990s might be attributable to long-term changes in lower stratospheric circulation. Such circulation changes may also have been responsible, at least in part, for the increase that has been observed at these latitudes since the mid-1990s. It is important to recognize that these empirical studies are correlative and statistical in scope, and so are only proxies for actual ozone transport.

Estimates of the dynamically induced contributions to ozone interannual variability and trends can be derived by using chemical transport models (CTM) driven by observed temperature and wind fields (Hadjinicolaou *et al.*, 1997; 2002; 2005). Using the SLIMCAT three-dimensional (3-D) CTM, Hadjinicolaou *et al.* (2005) found that about one-third of the observed ozone trend from 1979 to the mid-1990s could be explained by transport-related changes. In addition, Hadjinicolaou *et al.* (2005) also found that all of the midlatitude "increase" (see the period from the mid-1990s to 2004 in top right panel of Figure 3.3) could be explained by transport alone, and not by halogen decreases. However, the interannual variation discrepancies between CTMs and observations are large, making it difficult to place much weight on CTM results to attribute long-term transport changes.

The midlatitude ozone is influenced by polar loss via air mass mixing after the polar vortex breakup in early spring. Using regression analysis, Dhomse *et al.* (2006) concluded that this mechanism is one of the main factors responsible for the recent increase in Northern Hemisphere total ozone.

3.2.3.2 Chemistry

3.2.3.2.1 Polar chemistry

Heterogeneous reactions on PSCs convert the comparatively unreactive chlorine reservoirs hydrochloric acid (HCl) and chlorine nitrate ($ClONO_2$) first to chlorine gas (Cl_2) in the long, dark polar night. As soon as the Sun first appears over the horizon in the Antarctic spring in August each year, the Cl_2 photolyzes (breaks apart into chlorine atoms in the presence of sunlight, $Cl_2 + h\nu \rightarrow 2\ Cl$) and Cl atoms react with ozone to make chlorine monoxide (ClO) (see reaction 3c in Section 3.1). These reactions are often called "chlorine activation," since the chlorine compounds are converted from comparatively unreactive forms to much more photochemically reactive forms. At high concentrations, ClO reacts both with itself (reaction 3a forms the ClO dimer, dichlorine peroxide [ClOOCl], a reaction that actually proceeds faster at lower temperatures) and with the analogous bromine monoxide, BrO (see reaction 4a). Almost all of the rapid ozone loss in the Antarctic spring is attributed to catalytic cycles formed from the reaction of ClO with itself (reactions 3) and with BrO (reactions 4) (Frieler *et al.*, 2006).

Thus, stratospheric chlorine levels provide the fundamental driver for polar ozone loss, since chlorine is involved in the principal catalytic cycles responsible for polar ozone loss. Beyond this basic understanding, however, the calculated chemical loss rates of polar ozone are still quantitatively uncertain. Questions remain to be resolved on the photolysis rate of the ClOOCl (Equation 3b) and the balance between ClO and ClOOCl in the Antarctic stratosphere and the atmospheric abundance of bromine. Higher levels of bromine would improve the comparison between theory and observation for Arctic and Antarctic loss rates, but the exact sources of the extra bromine are somewhat uncertain.

From *in situ* aircraft measurements, Stimpfle *et al.* (2004) suggested that the ClO dimer cycle (reactions 3) may be a more efficient process for polar ozone loss than previously thought (Frieler *et al.*, 2006), and good overall consistency between *in situ* observations of ClO and the ClOOCl and model calculations can be achieved if it is assumed that ClOOCl photolyzes faster than assumed in WMO (2003). However, one recent laboratory study of the absorption cross-section of ClOOCl does not support this. It indicates that ClOOCl may photolyze (Equation 3b) slower than previously understood (Pope *et al.*, 2007). However, this slower photolysis rate results in severe underestimates by photochemical models of observed O_3 depletion rates and observed ClO levels, and hence poor representations of the severity of polar ozone losses (von Hobe *et al.*, 2007). Current models (without Pope *et al.*, 2007) reproduce the basic features of the Antarctic ozone hole and Arctic ozone losses using previous laboratory recommendations for photochemical parameters (*e.g.*, WMO, 2003; WMO, 2007). Clearly, more work will be required to understand this discrepancy.

Bromine may play a more important role in polar ozone depletion than previously thought.

Recent measurements show that bromine exists in the stratosphere at higher concentrations than is found in most 3-D models (WMO, 2007 and references therein). Profiles of BrO measured in the Arctic vortex suggest that inorganic bromine levels may be 3 to 8 parts per trillion (ppt) by volume larger than the amount of bromine carried to the stratosphere by methyl bromide (CH_3Br) and halons alone (Canty *et al.*, 2005; Frieler *et al.*, 2006). Although still uncertain, the additional 3-8 ppt of bromine is probably derived from very short lived (VSL) species containing bromine that enter the stratosphere at the tropical tropopause (WMO, 2007). Considering that the BrO + ClO cycle is now estimated to contribute up to half of total chemical loss of polar ozone, using the more efficient ozone loss by the ClO dimer cycle, this observation indicates the BrO + ClO catalytic cycle is likely to be a more efficient ozone loss process than considered in WMO (2003). Hence, bromine may play a more important role in polar ozone depletion than previously thought.

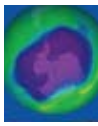

Polar stratospheric clouds are critically important in ozone photochemistry primarily through two processes: chlorine activation and denitrification. The chlorine heterogeneous reactions and sunlight lead to chlorine activation, while removal of nitric acid (HNO_3) occurs as PSCs fall out of the lower stratosphere and remove nitrogen, or denitrify, that air. Satellite observations of aerosols and clouds

in the polar stratosphere began with NASA's Stratospheric Aerosol Monitor (SAM) II in 1978, and continued nearly uninterrupted to 2005. These measurements used solar occultation in the visible and shortwave infrared portion of the electromagnetic spectrum. In addition to SAM II, other instruments included the NASA series of Stratospheric Aerosol and Gas Experiment (SAGE) I-III and the Naval Research Laboratory's Polar Ozone and Aerosol Measurement (POAM) II-III.

Models predict that the decline in ozone outside the polar regions should have ceased and that the next few decades should show the beginning of a recovery from the maximum depletion.

As noted in Section 3.2.3.1.1, V_{PSC} is a key parameter for estimating ozone loss. It is important to recognize that V_{PSC} actually represents the volume of temperatures cold enough to form PSCs, not the actual PSC volume over the polar region. Nevertheless, temperatures are directly related to PSC occurrence frequency (Steele *et al.*, 1983). The long-term PSC statistics are presented in Figure 3.13 (Fromm *et al.*, 2003). Here the PSC frequency (the number of profiles with a PSC divided by the number of profiles inside the polar vortex) for entire winter seasons is shown. In the Antarctic, PSCs are more frequent than the Arctic (Fromm *et al.*, 2003). There are large interannual variations in Antarctic PSC frequency but no obvious long-term trend. In the Arctic, as described in Section 3.2.2.2, stratospheric temperatures exhibit large variability and the average temperature is close to the PSC formation threshold temperature. In warm Arctic winters, little or no PSC activity is evident (for example, in the winter of 1984/1985). However, even in the coldest Arctic winters, PSCs only reach a 25% frequency.

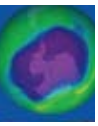

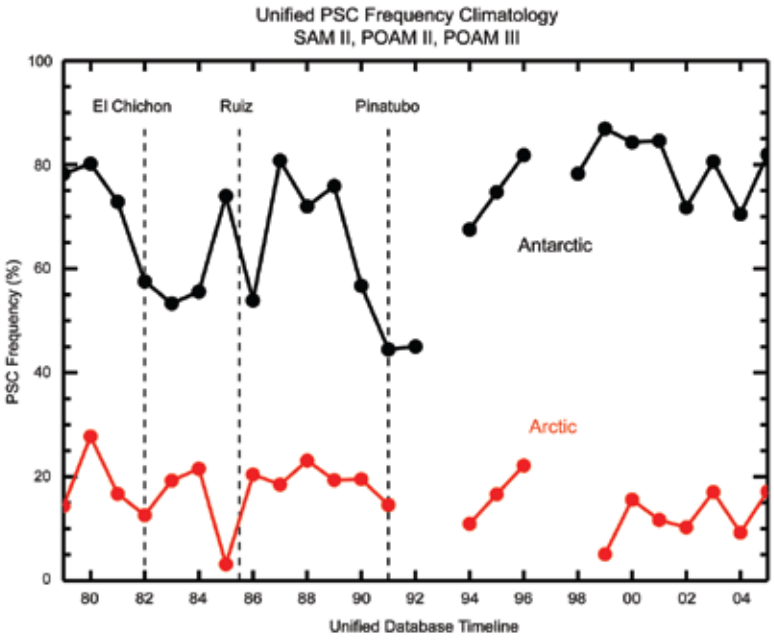

Figure 3.13 PSC frequency for the entire winter season. The frequency is calculated as the number of profiles with a PSC divided by the number of profiles inside the polar vortex. See Fromm *et al.* (2003) for details.

3.2.3.2.2 Global and midlatitude chemical processes

As in the polar regions, halogen increases (chlorine and bromine) have been the principal driver of ozone depletion over the past few decades in the midlatitudes. There is good overall agreement between observed long-term changes in ozone outside of the polar regions and model simulations that include the effects of increasing halogens. The models generally reproduce the observed ozone changes as a function of altitude, latitude, and season, confirming our understanding that halogen changes are the main drivers of global ozone changes (WMO, 2007). These models predict that the decline in ozone should have ceased and that the next few decades should show the beginning of a recovery from the maximum depletion. This is supported by the statistical fit of globally averaged ozone observations with Equivalent Effective Stratospheric Chlorine (EESC), a quantity that peaked in the late 1990s (Figure 3.2).

The explosive eruption of Mt. Pinatubo in 1991 injected large quantities of sulfur into the stratosphere (Trepte *et al.*, 1993). The sulfur-enhanced stratospheric sulfate aerosols provided significantly more surfaces that could support heterogeneous chemical reactions, thus converting a higher fraction of stratospheric chlorine to catalytically active forms. The impact of aerosols on midlatitude ozone was greatest in the early 1990s after the eruption of Mt. Pinatubo in 1991 (Figure 3.3). The observed decrease in Northern Hemisphere column ozone in 1993 agrees with chemical dynamical models that include these effects (WMO, 2003, 2007). The same models predict that the aerosols from Mt. Pinatubo should have produced a significant decrease in ozone over midlatitudes of the Southern Hemisphere, but no effect has been seen in either satellite measurements or ground measurements at stations such as Lauder, New Zealand.

The inclusion of additional inorganic bromine (Br_y) from very short-lived substances (VSLS) in models leads to larger ozone destruction at midlatitudes, compared with studies including only long-lived bromine source gases (*e.g.*, Salawitch *et al.*, 2005; Feng *et al.*, 2007b). The enhanced ozone loss occurs in the lower stratosphere via interactions of this bromine with anthropogenic chlorine. Midlatitude ozone loss is primarily enhanced during periods of high aerosol loading. The impact on long-term midlatitude ozone trends (1980-2004), assuming constant VSLS Br_y, is calculated to be small because aerosol loading was low at the start and end of this time period.

The profile of upper stratospheric ozone trends from 1980-2004 is generally consistent with our understanding of gas-phase chlorine chemistry as the cause of declining ozone, modulated by changes in temperature and other gases such as methane (WMO, 2007). However, global dynamical-chemical models have not demonstrated that they can simultaneously reproduce realistic trends in all relevant parameters, although observations over the full time period are limited (Eyring *et al.*, 2006). Chemical models without interactive radiation obtain ozone changes that peak at about 14% for 1980-2004 (in altitude coordinates), consistent with SAGE observations.

Our ability to reproduce observed past changes in the Northern Hemisphere is better than that for the Southern Hemisphere. Two-dimensional (2-D) models show large model-model differences in the Southern Hemisphere due to different treatments of the Antarctic ozone loss and how it is spread to the midlatitudes. Three-dimensional CTMs are inherently better at simulating the polar regions and this leads to smaller model-to-model differences. These CTMs, however, still do better at reproducing long-term changes in the Northern Hemisphere than in the Southern Hemisphere (WMO, 2007). This ongoing disagreement between model-observation comparisons in the Northern versus the Southern Hemisphere indicates that we do not yet have a full understanding of the combined chemical and transport processes controlling ozone changes at midlatitudes.

3.3 ULTRAVIOLET RADIATION AT THE EARTH'S SURFACE

3.3.1 Background (Factors Controlling UV Surface Irradiance)

Reductions in ozone lead to increases in ultraviolet (UVB) radiation at the Earth's surface. Higher UVB radiation can increase skin irritation.

The amount of UV radiation reaching the Earth's surface is controlled by several key factors including cloud cover, aerosols, and amount of atmospheric ozone (with most of the ozone being in the stratosphere). Ozone and cloud cover are the most important atmospheric components limiting the amount of UVB (280 to 315 nm) radiation able to reach the ground. Clouds and scattering aerosols reduce UV radiation at all wavelengths by reflecting a fraction of UV energy back to space, whereas ozone absorbs a fraction of the UV radiation only in the 280 to 340 nm range, with more absorption at shorter wavelengths than at longer wavelengths. Under special conditions, clouds can locally increase UV from 1% to 10% by cloud edge reflections. Extremely heavy cloud cover (black thunderstorm) can decrease UV almost 100%. Radiation with wavelengths shorter than 280 nm does not reach the surface in significant amounts because of absorption by the atmosphere (O_3 and O_2). Air pollution is an additional factor that can affect UV reaching the surface through the absorption and scattering by aerosols and absorbing trace gases such as tropospheric O_3 and nitrogen dioxide (NO_2). UV radiation at the surface is generally highest near the equator following the seasonally changing sub-solar point (latitude between ±23°), where stratospheric ozone is a minimum and the solar zenith angle (SZA) is the smallest. Larger amounts of UV radiation are seen at high altitude sites, especially those with predominantly dry and clear weather and large surface reflectivity (*e.g.*, from snow or ice cover). Understanding, modeling, and measuring the factors affecting the amount of UV radiation reaching the Earth's surface is important, since increases in UV radiation affect human health adversely through skin cancer (Diffey, 1991), eye cataracts (Taylor, 1990), and suppression of the immune system (Vermeer *et al.*, 1991), and positively through increased Vitamin D production (Grant, 2002; Holick, 2004). Changes in UV radiation also have important effects on ecosystem biology (Smith *et al.*, 1992; Ghetti *et al.*, 2006).

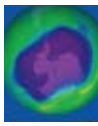

Both theory and observations (Figures 3.14 and 3.15) show that reductions in ozone lead to increases in UV erythemal radiation and UVB at the Earth's surface. Erythemal radiation is a weighted average of UVA (315 to 400 nm) and UVB used as a measure of skin irritation caused by exposure to sunlight (McKinlay and Diffey, 1987). The UV erythemal irradiance data shown in Figure 3.14 was obtained under clear-sky conditions at Mauna Loa, Hawaii, and shows the measured inverse relationship between ozone change and UVB radiation, which is the dominant portion of erythemal radiation. The relation to UV index and the units for

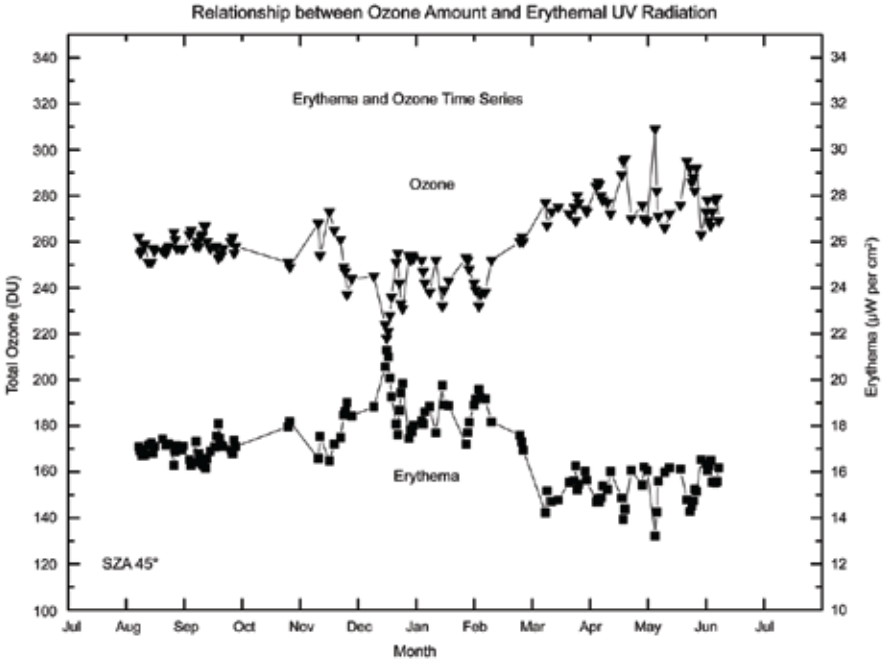

Figure 3.14 Measured erythemal irradiances (lower curve) from an ultraviolet spectroradiometer at SZA 45° compared with total ozone (upper curve) for 132 clear mornings during July 1995 to July 1996 at Mauna Loa Observatory (19.5°N, 155.6°W, 3.4 km), showing the inverse relationship between erythemal UV and ozone amount (adapted from WMO, 1999). (UV index 10 = 25 μW per cm^2 = 250 mW per m^2)

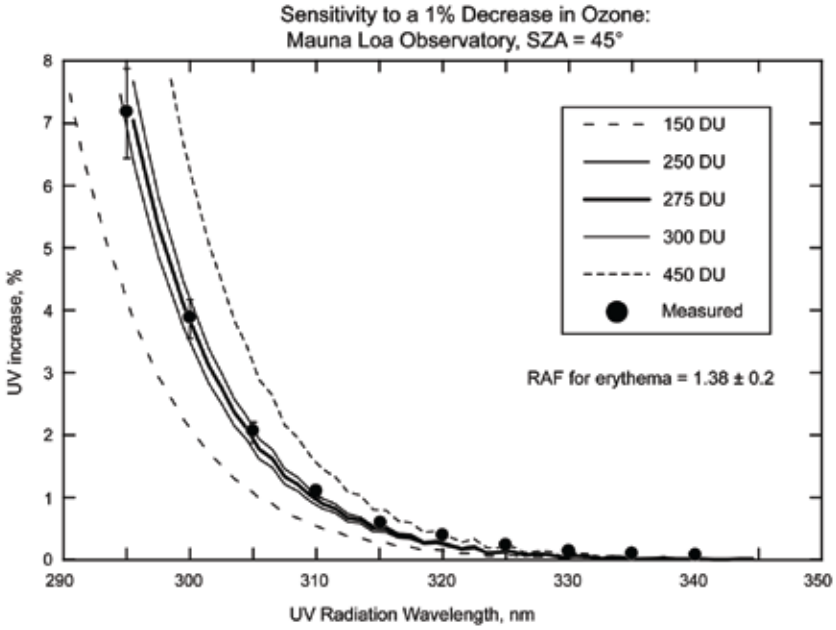

Figure 3.15 Validation of Equation 1 using the measured (dark circles) changes in ozone and UV irradiance from Mauna Loa, Hawaii, shown in Figure 3.14 (adapted from WMO, 1999).

irradiance and dose are discussed in Appendix 3B.

Increases in 280 nm to 340 nm UV radiation caused by decreases in ozone are easily estimated using radiative transfer calculations. For clear-sky conditions, the changes can also be accurately estimated using a simple relation between ozone and irradiance given in Equation 1:

$$dF/F = -d\Omega/\Omega\ \alpha\Omega\ \sec(\theta) = -d\Omega/\Omega\ (RAF) \quad (1)$$

where the quantity $\alpha\Omega\ \sec(\theta)$ is known as the Radiation Amplification Factor (RAF).

The relationship is derived from the standard Beer's Law of irradiance F attenuation in an absorbing atmosphere, $F = F_0 \exp(-\alpha\Omega\ \sec(\theta))$, where Ω is the ozone column amount in Dobson Units (DU, equal to milli-atm-cm), α is the ozone absorption coefficient (in cm^{-1}), θ is the solar zenith angle, and F_0 is the irradiance at the top of the atmosphere (Madronich, 1993). An example to show the magnitude of the RAF as a function of wavelength is shown in Figure 3.16 for $\theta = 45°$ and $\Omega = 330$ DU = 0.33 atm cm. The RAF method accurately estimates UV irradiance change compared to clear-sky radiative transfer (Herman *et al.*, 1999b). For example, radiative transfer shows that a 1% decrease in O_3 produces a 2.115% increase in 305 nm irradiance, while the RAF method estimates a 2.064% increase (Ω = 375 DU, θ = 30°). Changes in measured erythemal irradiance are approximated very accurately using Equation 1 with an RAF = 1.38 when the ozone amount changed by 1% (Figure 3.14, $\Omega = 275$ DU, $\theta = 45°$). For most conditions, erythemal irradiance change with ozone change behaves roughly the same as 308 nm irradiance.

The RAF approximation is useful for mid-day during the spring, summer, and autumn at most latitudes. During summer solstice, Equation 1 applies up to 83° latitude. In the presence of constant attenuation by cloud cover or scattering aerosols, Equation 1 still approximately gives the fractional change in irradiance for a change in ozone amount.

Fioletov *et al.* (1997) reported an extensive analysis of UVB irradiance and its dependence on total ozone. The analysis provides an empirical wavelength-by-wavelength measure of the increase of UVB irradiance for a 1% decrease of total ozone. These values were found to be essentially the same for clear and cloudy conditions (except for very heavy clouds) and are in good agreement with model results for longer wavelengths and moderate SZA.

UV radiation reaching the Earth's surface varies on all time scales, from seconds to seasons. Hourly to daily changes, *i.e.*, the short-term variations, are mostly due to cloud cover changes and aerosols, and to ozone in the UVB range. The extent of cloud cover also causes changes on daily and monthly time scales as the weather changes. In today's atmosphere, the multi-year variations are controlled principally by changes in stratospheric ozone, changes in the extent of cloud cover, and other longer-term changes such as in the amount of aerosol and

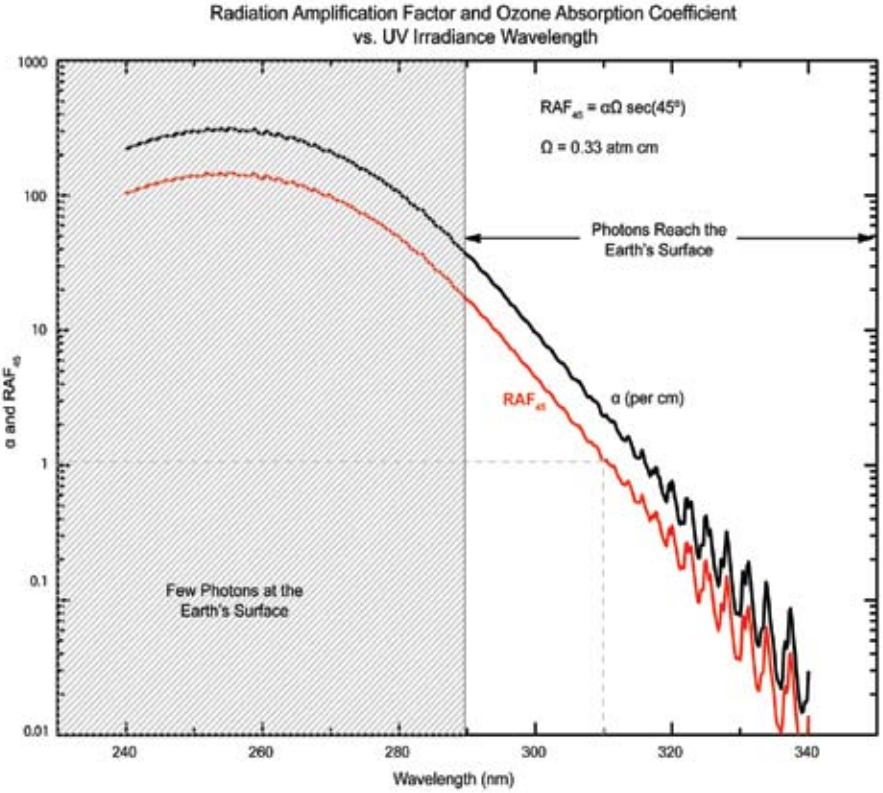

Figure 3.16 Ozone absorption coefficient α (cm^{-1}) and the Radiation Amplification Factor RAF_{45} for a solar zenith angle SZA = 45° and ozone amount of 330 DU (Ω = 0.330 atm cm). Note that at 310 nm the RAF_{45} is approximately 1, so that a 1% increase in O_3 would produce a 1% decrease in 310 nm irradiance.

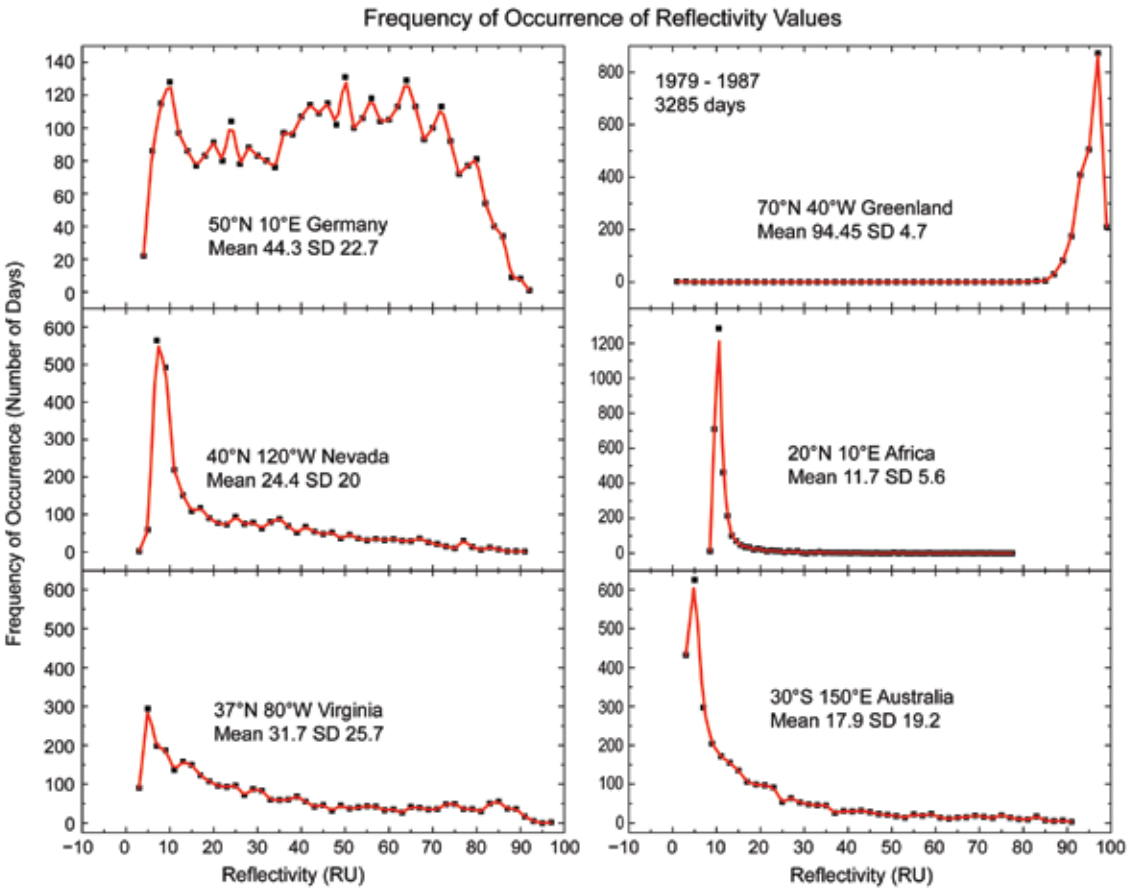

Figure 3.17 Frequency of occurrence of reflectivity values from 1979 to 1987 (3285 days) for six different locations. The mean and standard deviation (SD) are in RU (1 RU = 1%). Based on Herman *et al.* (2001a).

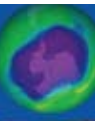

pollution. Day-to-day ozone-caused changes can be significant, but are usually smaller than changes due to cloud cover, because the stratospheric abundance of ozone only changes as a small percentage of its seasonally changing mean value. On longer time scales (decadal) most regional changes in cloud cover have been small (Herman *et al.*, 2008), so that global and zonal average changes in UVB due to long-term ozone depletion are dominant. In some regions (*e.g.*, northern Europe), decadal-term cloud changes are also important.

Ozone data from Nimbus-7/TOMS, obtained during June for the entire 5° longitudinal zone centered at 40°N, shows that the ozone amount can vary by 50 DU about the mean value of 350 DU, or $d\Omega/\Omega = \pm 0.14$. The day-to-day June ozone variation is obtained from figures similar to those shown in Herman *et al.* (1995). Using an average noon SZA for June of about 23° and an ozone absorption coefficient for 305 nm $\alpha = 4.75\ cm^{-1}$ yields a typical 305 nm irradiance change $dF/F = -d\Omega/\Omega\ \alpha\Omega\ \sec(\theta) = \pm 0.14 * 4.75 * 0.35 * 1.09 = \pm 0.25$. In other words, for clear-sky conditions, the 305 nm irradiance typically changes by ±25% during June just from to day-to-day ozone changes. As will be discussed later, the day-to-day variability of clear-sky 40°N UV June irradiance is about three times larger than the change caused by the long-term June decrease in ozone from 1980 to 2007 ($d\Omega/\Omega \sim -0.04$).

Identification of long-term (decadal) changes from ground-based measured surface UV radiation due to stratospheric ozone depletion can be accomplished if the data are filtered to remove the effects of clouds. Trend detection from ground-based measurements under all sky conditions, though appealing and relevant, has many difficulties. This is primarily because the surface UV is highly variable, as noted above, due to factors such as cloud cover and aerosols, and because the stratospheric ozone depletion has been rather small (less than 10%) over the past decades, with the exception of high latitudes (greater than 60°).

Other factors, such as Rayleigh scattering and surface reflectivity, affect the magnitude of measured or theoretically estimated UV irradiance. However, these factors do not significantly affect the short- or long-term changes in irradiance, since their changes are small. Hourly or daily changes in Rayleigh scattering follow the small changes in atmospheric pressure, which usually are less than 2%. There have been no long-term changes in mean atmospheric pressure. The UV surface reflectivity, R_G, is small (3 Reflectivity Units, RU, to 10 RU, where 1 RU = 1%) and almost constant with time except in regions seasonally or permanently covered with snow or ice. Based on radiative transfer studies, clear-sky atmospheric backscattering to the surface contributes less than 0.2 R_G to the measured UV irradiance, which is quite small for most ice/snow-free scenes.

3.3.1.1 Reduction of UV by Clouds

A measured daily cycle of UV reaching the surface will show large UV irradiance reductions from clear-sky conditions as clouds pass over a site. These reductions are frequently in excess of those caused by measured ozone changes from climatological values for wavelengths longer than 305 nm. In general, the effect of clouds is to reduce the UV amount at all wavelengths reaching the Earth's surface. The average amount of UV radiation reduction by clouds can be estimated from the Lambert Equivalent cloud reflectivity R, which varies significantly between locations (Figure 3.17). The operational definition of R is given in Appendix 3A.

Satellite data (Figure 3.17) show that the most commonly occurring values of R are about 3 to 5 RU greater than the surface reflectivity representing haze or very sparse cloud cover. Central Europe, represented by Germany, is quite different from North American sites in that the most frequent values are around 10 RU (127 days out of 3285 days) and around 50 RU (128 days), with almost the same number of days (80 to 128 days) having 10 to 70 RU. Greenland is another extreme, where the reflectivity is always high because of the ice cover. Nevada and Virginia are similar, except that Nevada has a lower average reflectivity representing less cloud cover. An extreme case is represented by Australia, where the average reflectivity (due to cloud cover) is very low and cumulative UV exposure is high compared to the same latitude in the United States.

Satellite observations of reflected UV indicate that reflectivities for typical midlatitude cloud-covered scenes have a wide range of values, which can reach 90 RU over high altitude cloud tops that occur most frequently in the tropics. Under snow-free conditions, the surface reflectivity R_G is usually between 2 RU and 4 RU, reaching about 10 RU in the Libyan Desert and similar small areas (*e.g.*, Andes Mountain high deserts). Area-averaged clear-sky UV surface irradiance is then approximately reduced as a linear function of the cloud plus aerosol reflectivity, which can be written in terms of effective transmission (Krotkov *et al.*, 2001), $T \approx (1 - R)/(1 - R_G)$, with local values occasionally exceeding clear-sky irradiances by about 10% because of reflections from the sides of clouds. Midlatitude UV irradiance reductions caused by clouds range up to 50%, which is larger than the day-to-day 305 nm UV variability caused by ozone (25%), and comparable to the change at 300 nm.

Snow-covered scenes cannot be distinguished from cloud cover by observations in the UV wavelengths. Because of this, the use of reflectivity to estimate the amount of UV radiation at the surface in the presence of snow is likely to be in error. For example, the very high reflectivity values observed in Greenland (Figure 3.17) are almost independent of the cloud cover.

Long-term changes in regional cloud and aerosol reflectivity must be considered when estimating long-term changes in UV irradiance. However, for most populated regions of the Earth, long-term (decadal) cloud and aerosol scattering changes have been shown to be small even where they are statistically significant (Herman *et al.*, 2001b, 2008). Local values of aerosol amounts and absorption are currently estimated from the widely distributed AERONET network of ground-based sunphotometers (Holben *et al.*, 2001).

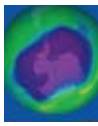

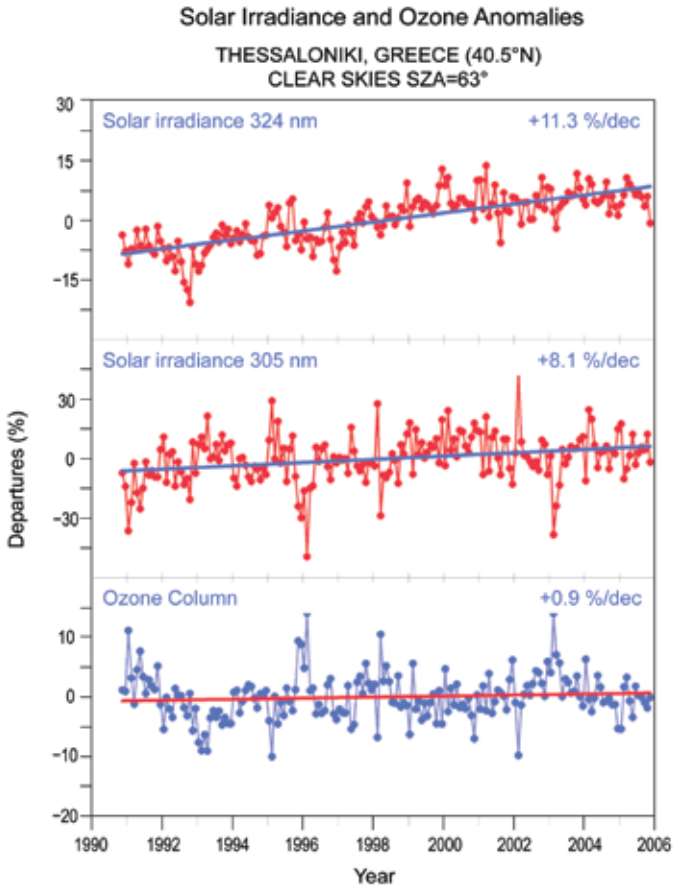

Figure 3.18 Combined effects of ozone, aerosols, and other absorbing components on UV radiation. Long-term variability in monthly mean solar spectral irradiances at 324 nm (upper panel) and at 305 nm (middle panel) measured at Thessaloniki, Greece, under clear skies at 63° solar zenith angle, shown as departures from the long-term (1990-2006) averages. The lower panel shows the corresponding departures in the ozone column of 375 DU (adapted from WMO, 2007).

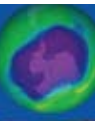

3.3.1.2 UV ABSORPTION

The amount of UV reaching the surface can also be affected by air pollution, *i.e.,* absorption by aerosols (black carbon, dust, and smoke), tropospheric O_3, NO_2, and other gases. These can cause reductions in UV of up to 10% in polluted sites, but with much higher reductions occurring in certain highly polluted cities, *e.g.*, occasionally in Los Angeles and frequently in Beijing. Nitrogen dioxide causes small reductions mainly to UVA since its absorption cross-section peaks near 410 nm, but is still significant at 330 nm. Aerosols of most types have much weaker wavelength dependence and affect UV and visible radiation at all wavelengths. Pollution abatement, especially in highly polluted regions, can decrease the atmospheric reflectivity and absorption, which has the effect of increasing the amount of UV and visible light reaching the ground.

3.3.1.3 ESTIMATING UV TRENDS: GROUND-BASED

Instrumental requirements for making long-term UV irradiance measurements are well understood in terms of calibration and stability for both spectrometers and broadband radiometers. While useful work can still be done with broadband instruments, much more information can be derived from high spectral resolution spectrometers (*e.g.*, the global network of Brewer spectrometers represented in the United States by the NOAA-EPA network of single-grating Brewers <http://www.esrl.noaa.gov/gmd/neubrew>, the National Science Foundation/Biospherical network, and at NASA by a modified double-grating Brewer (Cede *et al.*, 2006). Long-term surface UV spectral irradiance measurements must be carefully made and analyzed to preclude variations due to clouds that could be mixed into UV trend estimates, or whose variability can mask the detection of small changes. If ground-based data are filtered for cloud-free observations, then UVB changes caused by changes in ozone amount are easily observed in multi-year data records. Aerosols and other forms of pollution can also produce apparent changes in UV irradiance that mask the effect of ozone changes. These can be taken into account if measurements are made simultaneously in the UVB range (*e.g.*, 305 nm) and outside of the ozone absorbing range (*e.g.*, 324 nm). The lack of ability to separate aerosol and pollution effects from ozone-induced changes limits the usefulness of broadband instruments (300 to 400 nm) for understanding the observed irradiance changes.

Radiometric and wavelength calibration of spectrometers used for trend estimates must be carefully maintained to detect the relatively small changes caused by ozone and aerosols. Making accurate spectral measurements is quite difficult, since the natural UV spectrum at the ground changes by several orders of magnitude from 300 to 400 nm. A slight wavelength misalignment can cause significant errors in the measured UVB irradiance amount. Wavelength misalignment is less important for integrated quantities such as the erythemal irradiance.

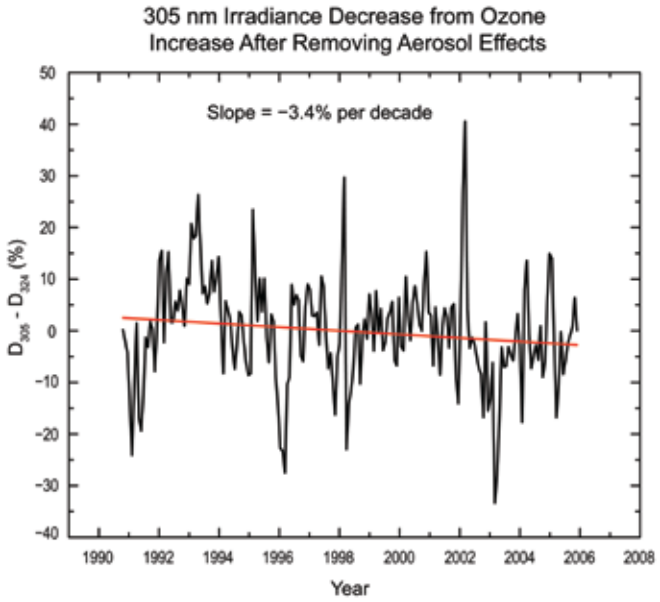

Figure 3.19 The difference between the 305 nm and 324 nm departures from the long-term (1990-2006) averages shown in Figure 3.18 showing the measured 3.4% per decade decrease in 305 nm irradiance caused by an ozone amount increase of 0.9% per decade.

A climatology of UV erythemal irradiance for the United States and Canada has been derived from Brewer and pyranometer data for the United States and Canada (Fioletov *et al.*, 2004). The ground-based climatology is lower by 10 to 30% than satellite estimates because of aerosol and pollution absorption that are neglected in the satellite estimates.

An excellent example of UV trend detection is from measured solar irradiances at 305 nm and 324 nm at Thessaloniki, Greece. The irradiances shown in Figure 3.18 are for cloud-free skies at a constant solar zenith angle of 63° (WMO, 2007, which are an extension of Bais and Lubin *et al.*, 2007). These data are obtained from a carefully maintained Brewer spectrometer located in an industrial area of Thessaloniki that is subjected to moderate amounts of pollution generated both locally and reaching Greece from other countries in Europe. There are also occasional dust episodes originating in northern Africa.

The radiation at 324 nm should not be significantly affected by ozone so that the cause of the upward trend at 324 nm (11.3% per decade) is almost certainly due to aerosol and pollution decreases. Decreasing amounts of aerosol and pollution that cause the upward trend at 324 nm will also affect 305 nm by approximately the same amount. Combining the changes seen for 324 nm with those observed for 305 nm (8.1% per decade) implies that the effect of increasing ozone amount (0.9% per decade) on 305 nm irradiance is a statistically significant decrease of 3.2% (11.3% minus 8.1%) per decade. This is also shown in Figure 3.19, where the time series for 324 nm, D_{324}, was subtracted from the time series for 305 nm D_{305}. The difference, $D_{305} - D_{324}$, was fit with a linear regression having a slope of –3.4% per decade.

An easy way to check this conclusion is through the radiation amplification factor defined as part of Equation 1. The radiation amplification factor, $RAF = -\alpha\Omega \sec(\theta) = -4$ for Ω=375 DU and θ=63°, the average measured values for Thessaloniki, Greece. Based on the RAF and the observed ozone change of 0.9% per decade, the change in 305 nm UV irradiance $dF/F = RAF\ d\Omega/\Omega$ should be approximately –4(0.9) = –3.6% per decade, consistent with the measurements of –3.2% and –3.4% per decade discussed above. In addition to the smaller ozone effects, Figure 3.18 shows that a decline in air pollutants can cause increases in surface UV irradiance of 11.3% per decade in a local industrial site such as Thessaloniki.

When data from cloudy and clear days are present in the UV time series, the measured trends in UV radiation at individual stations can have sufficient variation (typically 0 to 50%, and occasionally larger caused by clouds) to make estimated long-term trends lose statistical significance. As shown in the WMO (2007) report, trend estimates for the period from 1998 through 2005 for Toronto was 1.5±5% per decade (1 standard deviation, 1σ) (WMO, 2007) during a period in which the total ozone amount was relatively constant. Even using Toronto UV radiation data going back to 1990, no statistically significant trend is observable in the extended Toronto UV data despite ozone decreases that took place during the 1990s, because of variability introduced by clouds. To

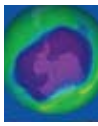

relate the estimated trends to ozone changes requires knowledge of changes in aerosol and cloud amounts, which can be obtained from a wavelength not affected by ozone.

3.3.1.4 Estimating UV Trends: Satellites

The data for estimating long-term changes of surface UV irradiance can come from individual local ground-based measurements or from global estimations using satellite ozone, aerosol, and cloud data. Global estimates of surface UV irradiance, UV_{EST}, as a function of latitude and longitude have been calculated from satellite measurements of atmospheric backscattered UV and the small amount reflected from the surface. UV_{EST} data are obtained from vector radiative transfer calculations that include polarization effects, ozone absorption, cloud reflectivity and transmission, aerosol scattering and absorption, and the measured surface reflectivity climatology (Herman and Celarier, 1997). The long-term precision and stability of a satellite instrument's in-flight calibration, especially the single channel radiances used to estimate cloud transmission and reflectivity, make it very useful for estimating trends in UV_{EST}. In the absence of a widely distributed closely spaced network of well-calibrated UV spectrometers, satellite UV irradiance estimates are extremely useful, especially over ocean areas where there are no other measurements. Since ozone amount, aerosol amount, and cloud reflectivity are the measured quantities, it is straightforward to separate their respective effects on estimated UV irradiance from satellite data.

There are two ways of estimating the UV irradiance reaching the ground from satellite ozone, aerosol, and reflectivity data. First, one can enter these quantities in a detailed plane parallel radiative transfer model to compute cloud transmission, C_T, using Mie theory to approximate the cloud and aerosol properties in addition to Rayleigh scattering and ozone absorption (Krotkov *et al.*, 1998; 2001). The second, and easier method, is to estimate the irradiance reaching the ground for a Rayleigh scattering and ozone absorbing atmosphere F_{CLEAR}, and then add the cloud and aerosol transmission as a correction factor based on the measured fractional scene R ($0 < R < 1$) and surface reflectivity R_G, $T \approx (1 - R)/(1 - R_G)$, where $0 < T < 1$. The irradiance at the surface is then approximately

$$F_{SURFACE} = T\, F_{CLEAR} \qquad (2)$$

The two methods agree quite closely (Krotkov *et al.*, 2001), except when there is enough multiple scattering within a cloud to give enhanced ozone absorption at wavelengths less than about 310 nm, where C_T is the better estimate. Both the C_T and the simplified method are frequently 10% higher than measured irradiance values on the ground, and sometimes 20% higher. The differences are usually caused by an underestimate in the satellite calculation of aerosol amount and aerosol absorption (Herman *et al.*, 1999a; Krotkov *et al.*, 1998; 2001; Kalliskota, 2000). The differences become much less when the aerosol amount is small or is known from ground-based measurements. Other sources of difference between ground-based measurements and satellite estimates of UV irradiance arise from the large satellite field of view (50 x 50 km^2 for TOMS and 12 x 24 km^2 for OMI) compared to the smaller ground-based field of view, and also from terrain height differences within a satellite field of view.

A recent comparison of measured UV erythemal irradiance from ground-based measurements and OMI satellite estimates has been made (Tanskanen *et al.*, 2007). The comparison shows that for flat, snow-free regions with modest loadings of absorbing aerosols or trace gases, the OMI-derived daily erythemal doses have a median overestimation of 0 to 10%, and 60 to 80% of the erythemal doses are within ±20% compared to ground-based measurements.

Similar errors occur when interpolating between widely separated ground-based stations, where the aerosol, ozone, and cloud amount varies between the stations. Given the need for global coverage of UV_{EST} and the sparsely located ground-based stations, calculations of UV_{EST} from satellite-observed column ozone abundances and cloud reflectivities, which are validated by ground-based measurements, are a useful method for estimating regional, zonal average, and global UV irradiance trends.

Note that year-to-year shifts in cyclic weather patterns (*e.g.*, clouds, ozone transport, *etc.*) by even a tenth of a degree in latitude and longitude (about 10 km) have a minimal effect on area-averaged satellite ozone and reflectivity measurements (and the UV estimates derived from them), but strongly affect ground-based UV measurements and their estimates of UV irradiance trends. Therefore, the surface UV changes deduced from ozone amounts and reflectivity measured by satellites, UV_{EST}, are expected to be equivalent to those from cloud-filtered ground-based observations of UV irradiance, and superior for estimating regional and global changes. Satellite measurements provide both local and global long-term coverage, which can be used to construct zonal and regional averages and long-term trends that have much less geophysical variance from clouds than corresponding ground-based measurements. The use of satellite estimates, however, presupposes ground-based measurements for validation and as a bridge between successive satellite instruments.

Satellite measures of UV_{EST} have used data from Nimbus7-TOMS (N7, 1979 to 1992), global weekly averages from multiple SBUV-2 instruments (1988 to present), global coverage from Earth-Probe TOMS (EP, 1997 to 2002), and the Aura satellite's Ozone Monitoring Instrument (OMI, 2005 to present). Other data are available from European satellites (*e.g.*, GOME).

It has been shown that cloud plus aerosol reflectivity over the United States has only changed by a small amount for the periods 1980 to 1992 (Herman *et al.*, 2001b) and for 1997 to 2007 (Herman *et al.*, 2008), where there are well-calibrated satellite reflectivity data records. Because of this, the change in UV irradiance over the United States can be estimated from just the change in satellite measured ozone amounts as shown in Figure 3.20. Fioletov *et al.* (2001) has made ground-based estimates of erythemal irradiance changes from two Brewer spectrometer stations (Montreal and Edmonton), and found that the UVB trends were similar to those expected from just changes in ozone, but with much larger uncertainty because of clouds and aerosols.

Satellite-observed long-term changes in ozone amount averaged over the United States suggest that there were significant UV changes for both erythemal irradiance and for UVB. Compared to the annual mean levels in 1980, the change in UV averaged over the United States was approximately 20% (erythemal irradiance) and approximately 40% (305 nm irradiance) early in 1993. Fortunately, these large percent changes were during the winter months when the solar zenith angles are large, so that the absolute irradiances are comparatively small. The calculated annual average irradiance increase during 1993 was about 7% and about 14% for erythemal and 305 nm irradiances, respectively. By 2007, the irradiance increase moderated to 4% and 8%, respectively, in response to a partial recovery of stratospheric ozone, which model calculations show is a direct consequence of the

Barrow, Alaska, has experienced UVB increases related to springtime ozone depletion, but these increases are a factor of ten smaller than those observed at the southern high latitudes.

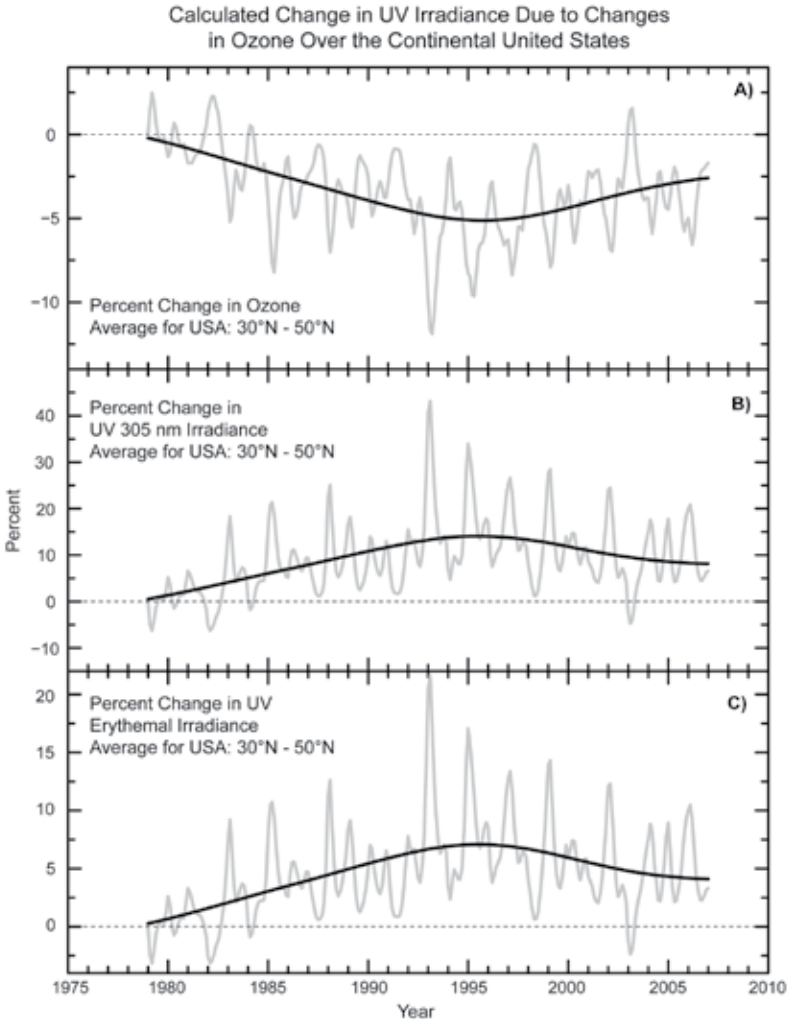

Figure 3.20 The calculated percent change in UV irradiance caused by percent changes in ozone over the continental United States. The ozone change is estimated from satellite measurements over the United States.

implementation of the Montreal Protocol and its subsequent Amendments.

3.3.2 UV in the Polar Regions

The expansion of the Antarctic polar vortex during the 1990s, both in spatial extent and temporal into early summer, has increased the frequency of elevated UVB episodes over sub-Antarctic populated areas. These episodes are no longer just small pockets of ozone-depleted stratospheric air coming from the breakup of the polar vortex, but include occasional excursions of the polar vortex edge over Ushuaia, Argentina and Punta Arenas, Chile. This occurred 44 times in the years 1997, 1998, and 2000 combined, with some episodes lasting three to four days. Surface measurements show average erythemal UV increases of about 70% over Ushuaia since 1997, and episodic total UVB increases of up to 80% over Punta Arenas (WMO, 2007 and references therein).

Diaz *et al.* (2003) show that Barrow, Alaska, has experienced UVB increases related to springtime ozone depletion in March and April, but these increases are a factor of ten smaller than those observed at the southern high latitudes. Summertime low-ozone episodes in the Arctic also affect surface UVB irradiances. These summertime events result from gas-phase chemistry involving nitrogen and hydrogen cycles, which become very efficient during the 24-hour insolation that occurs in the Arctic summer. During summer 2000, two low-ozone episodes brought about erythemal UV increases on the order of 10 to 15%, each lasting more than five days (WMO, 2007 and references therein).

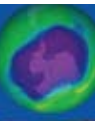

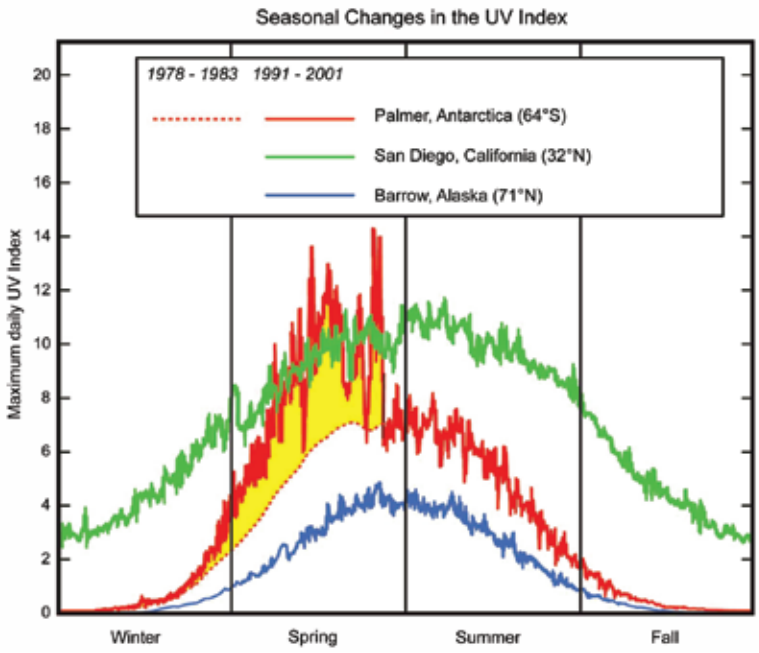

Figure 3.21 A comparison of measured erythemally weighted UV irradiance in Antarctica, the Arctic, and a midlatitude site in relative units. (Fahey, 2007)

Because of the extreme Antarctic springtime ozone depletion (ozone hole) compared to all other regions, it is useful to compare (Figure 3.21) the measured amounts of UV irradiance at Palmer Station, Antarctica (64°S) with San Diego, California (32°N) and Barrow, Alaska (71°N). For seasons other than spring in Antarctica, there is a decrease in UVB irradiance caused by the increased path through the atmosphere resulting in less UVB than in San Diego. The Antarctic ozone depletion that occurs each spring causes the UVB portion of the erythemally weighted irradiance to increase dramatically to where it exceeds even the summertime values observed in San Diego at 32°N. Similar wide-area springtime low ozone amounts do not occur in the Arctic region because of the degree of meteorological wave activity in the north that leads to a weaker polar vortex and higher ozone amounts.

3.3.3 Human Exposure to UV

From the viewpoint of human exposure to UV, the maximum clear-sky UV irradiance and exposure occurs in the equatorial zone, 23.3°S to 23.3°N, following the seasonal sub-solar point, and at high mountain altitudes. In general, UV erythemal, UVA, and UVB irradiance decreases with increasing latitude outside of the equatorial zone, since the maximum daily noon solar elevation angle decreases. An exception occurs for UVB wavelengths at southern mid- to high latitudes when reduced ozone amounts from the Antarctic ozone hole remain late into the spring and are pushed away from Antarctica towards lower latitudes, which includes some populated areas. For example, UV measurements indicate equatorial irradiance levels can occur in the southern part of South America for several days.

Global images of daily-integrated UV erythemal exposure (kilojoules, kJ per m^2) averaged during the months of January (Southern Hemisphere summer) and July (Northern

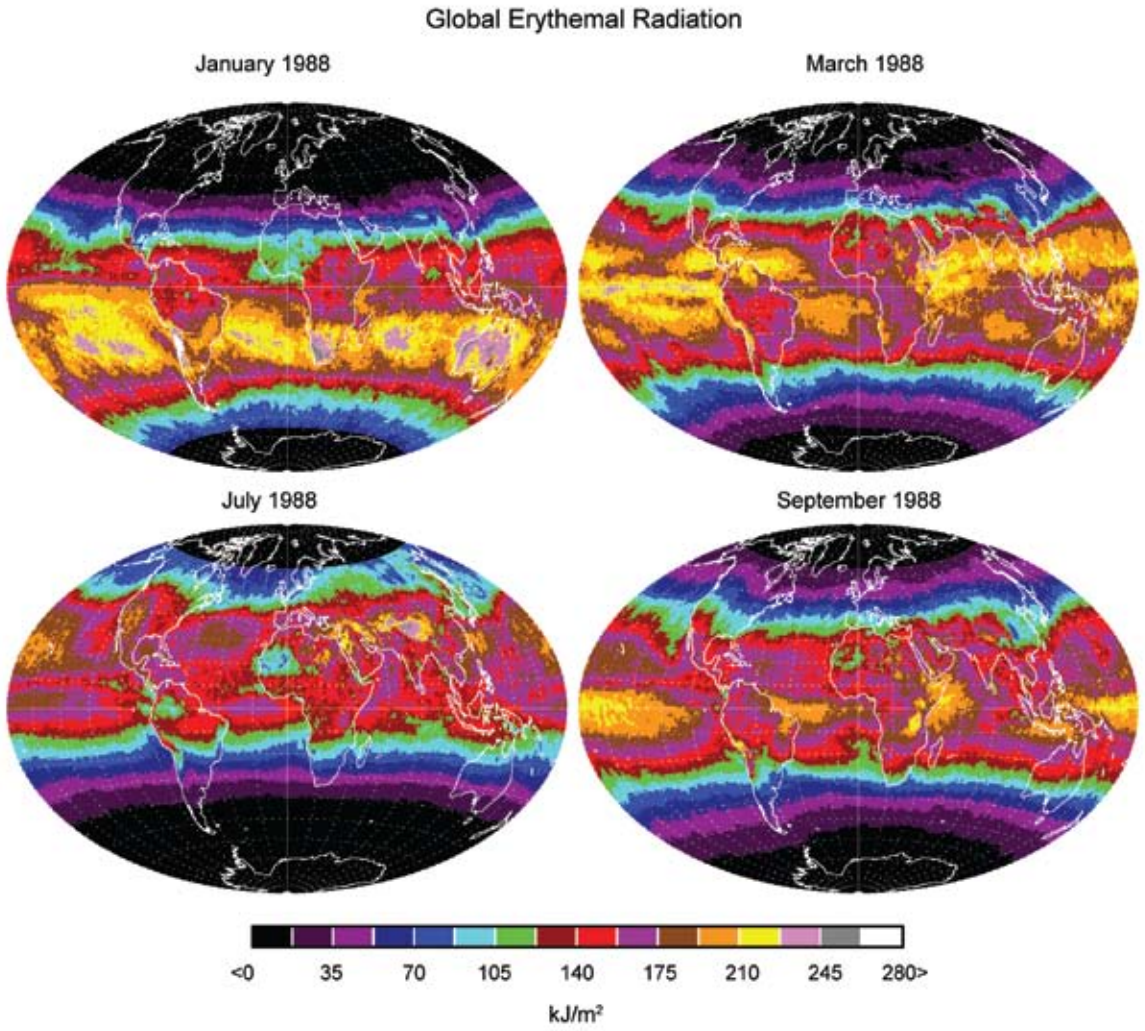

Figure 3.22 Erythemal exposure kJ per m^2 for the months of January, March, July, and September 1988 (from WMO, 1999) based on Nimbus-7/TOMS ozone and reflectivity data. In terms of the UV index, the numbers would be divided by 25. High UV levels are observed over Antarctica in the Southern Hemisphere late Spring and Summer (Figure 3.21). These extreme levels are not seen in the September 1988 panel because the sun is just beginning to rise over Antarctica and the 1988 ozone depletion was not extreme (Figures 3.5 and 3.7).

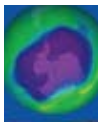

Hemisphere summer), and the two equinox months September and March, are shown in Figure 3.22 (based on WMO, 1999). Because of cloud cover, the high equatorial clear-sky irradiances do not translate into the highest monthly cumulative exposures. The maximum erythemal doses at the equator occur when the sun is directly overhead during March, which has lower cloud cover than during September. The difference is related to the annual cycle of the cloud cover associated with the Intertropical Convergence Zone (ITCZ), which is usually over the equator in September, but is south of the equator in March. Two extreme examples of very high UV exposures occur in the South American Andes (*e.g.*, the sparsely populated Atacama Desert in Chile at 4400 to 5600 meters altitude) during January and in the Himalayan Mountains (over 100 peaks exceeding 7000 meters in height) during July as shown in Figure 3.22. Excluding high altitude locations, the largest monthly UV exposures occur in Australia and South Africa during summer (January) because of their very low amount of day-to-day cloud cover from late spring to early autumn. Other midlatitude low altitude areas also receive high doses, *e.g.*, summertime (July) in the southwest United States and the Mediterranean countries.

The southwest United States receives high UV exposures during summertime.

Other factors contribute to the high Southern Hemisphere UV doses. There is a five million km decrease in Earth-Sun distance for the Southern Hemisphere summer solstices, as compared to the Northern Hemisphere, causing a 6.5% increase in summer solstice irradiance

Through the Montreal Protocol and subsequent agreements, CFCs were almost completely phased out by 1995, preventing major chlorine-driven ozone decreases and UVB increases.

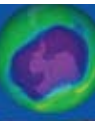

in the Southern Hemisphere. Average summer ozone in the Southern Hemisphere (270 DU) is lower than the Northern Hemisphere (320 DU) by about 13%, which would lead to a 13% increase in 310 nm and a 26% increase in 305 nm irradiance. The exact percent increase is a function of latitude. In general, the Southern Hemisphere has less pollution aerosols, which can cause another few percent increase in UV irradiance relative to Northern Hemisphere.

In Australia and South Africa, the combination of high UV exposure and residents of European descent have lead to a major skin cancer health problem. Based on National Institutes of Health data, the same problems are present in the United States, with more skin cancer occurring at lower latitudes where the UV exposure is higher. The seriousness of the very high UV exposure problem is observed in Australia, where skin cancer rates have increased dramatically (20% for basal cell, to 788 per 100,000; over 90% for squamous cell, to 321 per 100,000 carcinomas), based on household surveys conducted in 1985, 1990, and 1995 (Staples *et al.*, 1998). This compares to the U.S. National Cancer Institute estimate of 14.5 per 100,000 for the United States. Lucas *et al.* (2006) give a comprehensive review of health problems and benefits related to UV exposure.

3.3.4 UV Summary

Measurements from ground-based instruments at different midlatitude sites around the globe show a mixture of UVB increases and decreases that depend on changes in local cloud cover, ozone, and aerosol amounts. Trends in UV in the polar regions, especially Antarctica, are dominated by changes in springtime stratospheric ozone. In the latitude range 60°S to 60°N, all three main factors governing UVB must be taken into account (for UVA, clouds and aerosols are the dominant factors). Ground-based stations located in or near urban sites have observed increases in cloud-free sky UV radiation from pollution abatement comparable to those from observed total column ozone changes.

Measurements of ozone and cloud plus aerosol reflectivity from satellites have been used to estimate the changes in UVB over the last 28 years. Based on the satellite ozone record, the annual average clear-sky UV erythemal irradiance averaged over the continental United States increased from 1979 to the mid-1990s by about 7%. Since the mid-1990s the erythemal irradiance has decreased, so that the current level is about 4% higher than it was at the start of the record in 1979. Year-to-year and seasonal variations ranged from only a few percent to about 20% with the largest changes occurring during the winter months when UV irradiance is at an annual minimum. In the absence of the Montreal Protocol, summer maximum and annually integrated UVB doses over the United States would have been much larger with adverse consequences for public health and ecosystems (U.S. EPA, 1999).

Ground-based measurements of surface UV trends present a challenge that can be overcome with proper analysis of the data for cloud-free conditions along with simultaneous aerosol measurements. UV estimates from satellite measurements of ozone, aerosols, and cloud reflectivity are averages over large areas on the order of 25 km to 100 km, which minimizes many problems with local variability of cloud and aerosol amounts. Both ground and satellite UV estimates are critically dependent on establishing and maintaining an accurate calibration over the lifetime of an instrument and between successive instruments. Ground-based measurements are essential to provide validation of satellite calibration and as a bridge between successive satellite instruments.

While the UV irradiance maximum in 1993 was associated with the massive equatorial Mt. Pinatubo eruption in 1991, a portion of the total increase occurred before 1991 and was associated with ozone destruction from chlorine loading in the atmosphere before being limited by the Montreal Protocol. Major chlorine-driven ozone decreases and UVB increases were prevented by this and subsequent agreements that were effective for limiting releases of chloroflourocarbons (CFCs) and other chlorine-bearing compounds, with CFCs being almost completely phased out by 1995.

APPENDIX 3A: LAMBERT EQUIVALENT REFLECTIVITY (LER)

The Lambert Equivalent Reflectivity, R, is calculated by requiring that the measured radiance, I_{SM}, match the calculated radiance, I_S, at the observing position of the satellite (Equation A1) by solving for the single free parameter, R, in the formal solution of the radiative transfer equation

$$I_S(\Omega,\Theta,R,P_O) = \frac{RI_d(\Omega,\Theta,P_O)f(\Omega,\Theta,P_O)}{1-RS_b(\Omega,P_O)} + I_{dO}(\Omega,\Theta,P_O) = I_{SM} \quad \text{(A1)}$$

where Ω = ozone amount from shorter wavelengths (*e.g.*, 317 nm)
Θ = viewing geometry (solar zenith angle, satellite look angle, azimuth angle)
R = LER at P_O $\quad 0 < R < 1$
P_O = pressure of the reflecting surface (*e.g.*, ground or cloud)
S_b = fraction scattered back to P_O from the atmosphere
I_d = sum of direct and diffuse irradiance reaching P_O
f = fraction of radiation reflected from P_O reaching the satellite
I_{dO} = radiance scattered back from the atmosphere for R=0 and P=P_O

The quantities S_b, I_d, f, and I_{dO} are calculated from a radiative transfer solution and stored in tables. From Equation A1,

$$R = \frac{I_{SM} - I_{dO}}{I_d f + (I_{SM} - I_{dO})S_b} \quad \text{(A2)}$$

APPENDIX 3B: UV INDEX AND UNITS

Erythemal irradiance is frequently expressed in terms of the UV index = 25 milliWatts (mW) per m^2 = 2.5 microWatts (μW) per cm^2 (the units of Figure 3.14). The index is an arbitrary unit such that very high values reported by weather services have a UV index of 10. In Figure 3.14, the highest value is about 22 μW per cm^2, which is a UV index of 8.8. High altitude locations with extreme UV amounts can exceed 10 on clear days. Erythemal exposure or dose is a time-integrated quantity normally expressed in kJ per m^2.